PLOS PATHOGENS

RESEARCH ARTICLE

Exploiting bacterial effector proteins to uncover evolutionarily conserved antiviral host machinery

Aaron Embry[1], Nina S. Baggett[1], David B. Heisler[1], Addison White[1], Maarten F. de Jong[1], Benjamin L. Kocsis[1], Diana R. Tomchick[2], Neal M. Alto[1]*, Don B. Gammon[1]*

1 Department of Microbiology, University of Texas Southwestern Medical Center, Dallas, Texas, United State of America, **2** Department of Biophysics, University of Texas Southwestern Medical Center, Dallas, Texas, United State of America

* neal.alto@utsouthwestern.edu (NMA); don.gammon@utsouthwestern.edu (DBG)

Citation: Embry A, Baggett NS, Heisler DB, White A, de Jong MF, Kocsis BL, et al. (2024) Exploiting bacterial effector proteins to uncover evolutionarily conserved antiviral host machinery. PLoS Pathog 20(5): e1012010. https://doi.org/10.1371/journal.ppat.1012010

Editor: Harmit S. Malik, Fred Hutchinson Cancer Research Center, UNITED STATES

Received: January 31, 2024

Accepted: April 11, 2024

Published: May 16, 2024

Data Availability Statement: All relevant data are within the manuscript or supporting information (S5 Table). Structures for Ceg10 unmodified (PDB DOI: https://doi.org/10.2210/pdb9B8D/pdb; PDB ID: 9B8D) and Ceg10 S-nitrosylated (PDB DOI: https://doi.org/10.2210/pdb9B8E/pdb; PDB ID: 9B8E) have been deposited into the RCSB Protein Data Bank (PDB).

Funding: This work was supported by grants to DBG from the National Institutes of Health [NIH; https://www.nih.gov/] (1R35GM137978-01 and

Abstract

Arboviruses are a diverse group of insect-transmitted pathogens that pose global public health challenges. Identifying evolutionarily conserved host factors that combat arbovirus replication in disparate eukaryotic hosts is important as they may tip the balance between productive and abortive viral replication, and thus determine virus host range. Here, we exploit naturally abortive arbovirus infections that we identified in lepidopteran cells and use bacterial effector proteins to uncover host factors restricting arbovirus replication. Bacterial effectors are proteins secreted by pathogenic bacteria into eukaryotic hosts cells that can inhibit antimicrobial defenses. Since bacteria and viruses can encounter common host defenses, we hypothesized that some bacterial effectors may inhibit host factors that restrict arbovirus replication in lepidopteran cells. Thus, we used bacterial effectors as molecular tools to identify host factors that restrict four distinct arboviruses in lepidopteran cells. By screening 210 effectors encoded by seven different bacterial pathogens, we identify several effectors that individually rescue the replication of all four arboviruses. We show that these effectors encode diverse enzymatic activities that are required to break arbovirus restriction. We further characterize *Shigella flexneri*-encoded IpaH4 as an E3 ubiquitin ligase that directly ubiquitinates two evolutionarily conserved proteins, SHOC2 and PSMC1, promoting their degradation in insect and human cells. We show that depletion of either SHOC2 or PSMC1 in insect or human cells promotes arbovirus replication, indicating that these are ancient virus restriction factors conserved across invertebrate and vertebrate hosts. Collectively, our study reveals a novel pathogen-guided approach to identify conserved antimicrobial machinery, new effector functions, and conserved roles for SHOC2 and PSMC1 in virus restriction.

Author summary

Microbial pathogens such as viruses and bacteria encounter diverse host cell responses during infection. While viruses possess antagonists to counter these responses in natural

1R21AI169558-01A1) and by funding to DBG from the UTSW Endowed Scholars Program. NMA was supported by NIH National Institute of Allergy and Infectious Diseases (R01AI083359), The Welch Foundation [https://welch1.org/] (I-1704) and The Burroughs Welcome Fund [https://www.bwfund.org/] (1011019). This research was also supported with training grant funding from the NIH to AE, NSB, DBH (T32 AI007520). The funders had no role in study design, data collection and analysis, decision to publish, or preparation of the manuscript.

Competing interests: The authors declare that there are no competing interests.

host species, their replication can be restricted in unnatural host cells where their antagonists are ineffective. Bacteria also employ a diverse repertoire of immune evasion proteins known as "effectors" that can inhibit antimicrobial responses found in invertebrate and vertebrate hosts. In this study, we hypothesized that some bacterial effectors may target host immunity proteins that restrict both bacteria and viruses. To test this hypothesis, we screened a bacterial effector library comprising 210 effectors from seven distinct bacterial pathogens for their ability to rescue the replication of four viruses in insect cells that are normally non-permissive to these viruses. Though numerous effectors were identified to rescue the replication of each virus, the uncharacterized IpaH4 protein encoded by the human pathogen *Shigella flexneri* was able to rescue all four viruses screened. We discovered that IpaH4 enhances arbovirus replication in both restrictive insect and permissive human cells by directly targeting two novel, evolutionarily conserved antiviral host proteins, SHOC2 and PSMC1, for degradation. Our study establishes bacterial effectors as valuable tools for identifying critical antimicrobial machinery employed by eukaryotic hosts.

Introduction

Arboviruses comprise a diverse group of arthropod-borne viruses that are transmitted by dipteran (fly and mosquito) vectors to animal and human hosts. For example, vesicular stomatitis virus (VSV) is a negative-sense single-stranded (ss)RNA virus belonging to the *Rhabdoviridae* family that is the leading cause of vesicular disease in livestock in the United States, resulting in costly animal quarantines and trade embargoes [1]. Of the ~500 arboviruses that have been identified, ~150 are known to cause disease in humans [2]. Consequently, in 2022, the "Global Arbovirus Initiative" was launched by the World Health Organization to monitor and control arboviral disease [3]. Notable among arboviruses causing disease in humans are the positive-sense ssRNA viruses belonging to the *Togaviridae* family. This family includes chikungunya virus, the second-most prevalent arbovirus infecting humans worldwide [2]. However, the need for biosafety level (BSL)-3 facilities to culture wild-type strains of chikungunya virus poses significant challenges to studying this togavirus. In contrast, other less pathogenic togaviruses [e.g. Ross River virus (RRV), O'nyong'nyong virus (ONNV), Sindbis virus (SINV)], can be cultured under BSL-2 conditions and thus have become important models for understanding togavirus-host interactions [4,5]. However, we still lack vaccines and antiviral drugs to combat most human arbovirus infections, including those caused by togaviruses [5]. Thus, the identification of immune mechanisms that restrict arbovirus replication may provide additional avenues for the development of effective strategies to combat arboviral disease.

While genome-wide CRISPR-Cas9 and RNA interference (RNAi) screening platforms have been used to identify host immunity factors affecting arbovirus replication [6–8], these assays can be difficult, time-consuming, and cost prohibitive to set up, and are not easily applicable to non-model host systems. Moreover, these assays cannot provide insight into the strategies used by pathogens to combat host antiviral factors identified in these screens. Identification of pathogen-encoded immune evasion proteins (IEPs) targeting host immunity factors is important for several reasons. First, the existence of such IEPs is strong evidence for the physiologic importance of these interactions during the "molecular arms race" between pathogen and host. Second, while some IEPs simply bind/sequester host factors to inhibit their function, others can alter post-translation modifications to modify stability or function [9]. Thus, IEPs can be used as "tools" to both identify the host immunity factors they target and uncover molecular

mechanisms that regulate host factor function. Third, IEPs often drive virulence and thus their characterization can reveal pathogenesis mechanisms [10,11]. It is paramount to develop simplistic, functional assays that can both identify key antiviral factors restricting viral replication and that provide molecular tools to mechanistically dissect the function of such immunity factors.

Although arboviruses are well-adapted to replicate in dipteran and mammalian hosts, we have previously shown that several arboviruses, such as VSV and SINV, undergo abortive infections in cells derived from lepidopteran (moth and butterfly) hosts [12,13]. For example, in *Lymantria dispar* (spongy moth)-derived LD652 cells, VSV and SINV undergo abortive infections post-entry after limited gene expression. However, their replication can be rescued by global inhibition of host transcription or by expression of mammalian poxvirus-encoded IEPs termed "A51R proteins", suggesting that innate antiviral defenses block VSV and SINV replication in LD652 cells [12]. However, the host immune responses that are at play during restricted arboviral infections in LD652 cells remain poorly defined. More recently, we have reported the full genomic sequence of *L. dispar* and the LD652 cell transcriptome [14], making virus-LD652 cell systems more amenable to uncovering pathogen-host interactions at the molecular level. Our finding that mammalian poxviral IEPs can retain immunosuppressive function in LD652 cells suggests that some pathogen-encoded IEPs target host machinery conserved between insects and mammals. Thus, we were interested in identifying IEPs from other mammalian pathogens that promote arbovirus replication in LD652 cells. Such IEPs might be useful molecular tools in identifying the conserved host immunity factors they target.

Bacterial pathogens encode a wide array of IEPs that can manipulate eukaryotic immune responses. Many of these bacterial IEPs are "effector" proteins that are injected into eukaryotic host cells through bacterial secretion systems [10,15]. These effectors can manipulate, usurp, and/or inhibit a variety of cellular processes once inside the host cell cytoplasm including cytoskeletal dynamics, host signaling cascades, and innate immune responses [10,15]. Interestingly, some bacterial effectors inhibit innate immune pathways that are also antagonized by viruses, such as the Type I interferon (IFN) response [16], suggesting that bacterial and viral pathogens may need to evade common eukaryotic defense mechanisms. Although significant advances have been made towards understanding effector biology, the function of many effectors remains unknown. Understanding bacterial effector function is important because these proteins can be critical drivers of bacterial pathogenesis [10,15]. However, defining the role of individual effectors during infection can be challenging due to functional redundancy among independent effectors encoded by a single bacterial pathogen [17]. Therefore, experimental strategies to study effector functions outside of bacterial infections may be useful for determining their role during natural infection.

Here, we further explore the restricted infections of arboviruses in lepidopterans by infecting moth cells with the rhabdovirus, VSV, and the togaviruses: SINV, RRV, and ONNV. We develop a simple, yet innovative approach to uncover evolutionarily conserved antiviral factors through the identification of bacterial effectors that rescue arbovirus replication in LD652 cells. By expressing a library of 210 effector proteins encoded by seven distinct bacterial pathogens, we identify six effectors capable of rescuing all four restricted arboviruses in LD652 cells: SopB, IpgD, HopT1-2, HopAM1, Ceg10, and IpaH4. Using mutagenesis, we demonstrate the importance of diverse enzymatic functions for SopB, IpgD, HopAM1, and IpaH4 in breaking arbovirus restriction. Moreover, crystallography and cell cultures studies reveal Ceg10 to encode a putative cysteine protease function that is required for arbovirus rescue. By focusing on the *Shigella flexneri*-encoded effector IpaH4, we reveal this novel bacterial E3 ubiquitin ligase to directly target two conserved host proteins, SHOC2 and PSMC1, for degradation in moth and human cells. To our knowledge, roles for these host factors in virus restriction had not been reported in any eukaryotic system. However, we show that depletion of intracellular

SHOC2 or PSMC1 levels in moth or human cells promotes arbovirus replication, suggesting they have ancient roles in combating viral infection across diverse eukaryotic host species. Together, our findings demonstrate the utility of using naturally abortive arbovirus infections in lepidopteran cells for the interrogation of arbovirus-host interactions and establish it as a model for identifying conserved host immunity proteins targeted by pathogens.

Results

Inhibition of host transcription rescues restrictive arbovirus replication in LD652 cells

Previously, we showed that the normally abortive infection of VSV and SINV in LD652 cells can be rescued by treatment of cultures with actinomycin D (ActD), an inhibitor of transcription [12]. ActD globally blocks transcription by host DNA-dependent RNA polymerases by intercalating into GC-rich regions of cellular DNA and thus does not impede viral RNA-dependent RNA polymerase-mediated transcription [18,19]. The relief of arbovirus restriction by ActD treatment suggests that VSV and SINV undergo abortive infections in LD652 cells due to cellular antiviral responses that require active transcription [12]. To confirm these previous results and to determine if ActD treatment could relieve restriction of additional togaviruses related to SINV, such as RRV and ONNV, LD652 cells were infected with GFP reporter viruses (VSV-GFP [12], SINV-GFP [12], RRV-GFP [20], and ONNV-GFP [21]) in the absence or presence of ActD. Cells were then stained with CellTracker Orange Dye and imaged 72 h post-infection (hpi). Representative GFP fluorescence images and quantitative GFP signals (normalized to cell number with CellTracker signals) were used as a readout for viral replication and are shown in **Fig 1A and 1B**. As expected, 0.05 μg/mL ActD treatment increased GFP signal in VSV-GFP and SINV-GFP infections by ~10,000- and 100-fold, respectively (**Fig 1B**). Additionally, ActD treatment during VSV-GFP and SINV-GFP infection increased their viral titer by ~1,000-fold for both viruses (**Fig 1C**). During ONNV-GFP and RRV-GFP infections, ActD increased GFP signal and viral titer by ~100-fold and ~10-fold, respectively (**Fig 1A-1C**). Importantly, we have previously shown that LD652 cells treated with this dose of ActD retain ~90% viability [12], and thus enhanced virus replication is not due to a general decrease in cell viability. Together, these findings suggest that arbovirus infection of LD652 cells induces a restrictive immune response that requires active host transcription.

Specific bacterial effectors relieve arbovirus restriction in LD652 cells

We have previously shown that poxvirus-encoded A51R proteins are IEPs that rescue restricted arbovirus replication when expressed from plasmids transfected into LD652 cells [12,22]. Therefore, we asked if bacterial effector proteins, which often function as IEPs, could also rescue arbovirus replication. To do this, we adapted and expanded a previously described effector library for expression in insect cells [23]. Briefly, 210 secreted bacterial effectors from seven pathogens (*Shigella flexneri*, *Salmonella enterica* serovar Typhimurium, *Pseudomonas syringae*, Enterohemorrhagic *E. coli* O157:H7, *Yersinia pseudotuberculosis*, *Legionella pneumophila*, and *Bartonella henselae*) were cloned into the pIB/V5-His insect expression vector and screened for their ability to alleviate arbovirus restriction in LD562 cells. The pIB/V5-His-based effector library was transfected into LD652 cells for 48 h and then cells were infected with either GFP reporter viruses (RRV-GFP and ONNV-GFP) or luciferase reporter strains (SINV-LUC and VSV-LUC [12,22]) for 72 h (**Fig 2A**). After infection, reporter read-outs were measured and the "fold change" in GFP or luciferase signals was calculated by dividing values in effector treatments by the mean values obtained in cultures transfected with empty vector

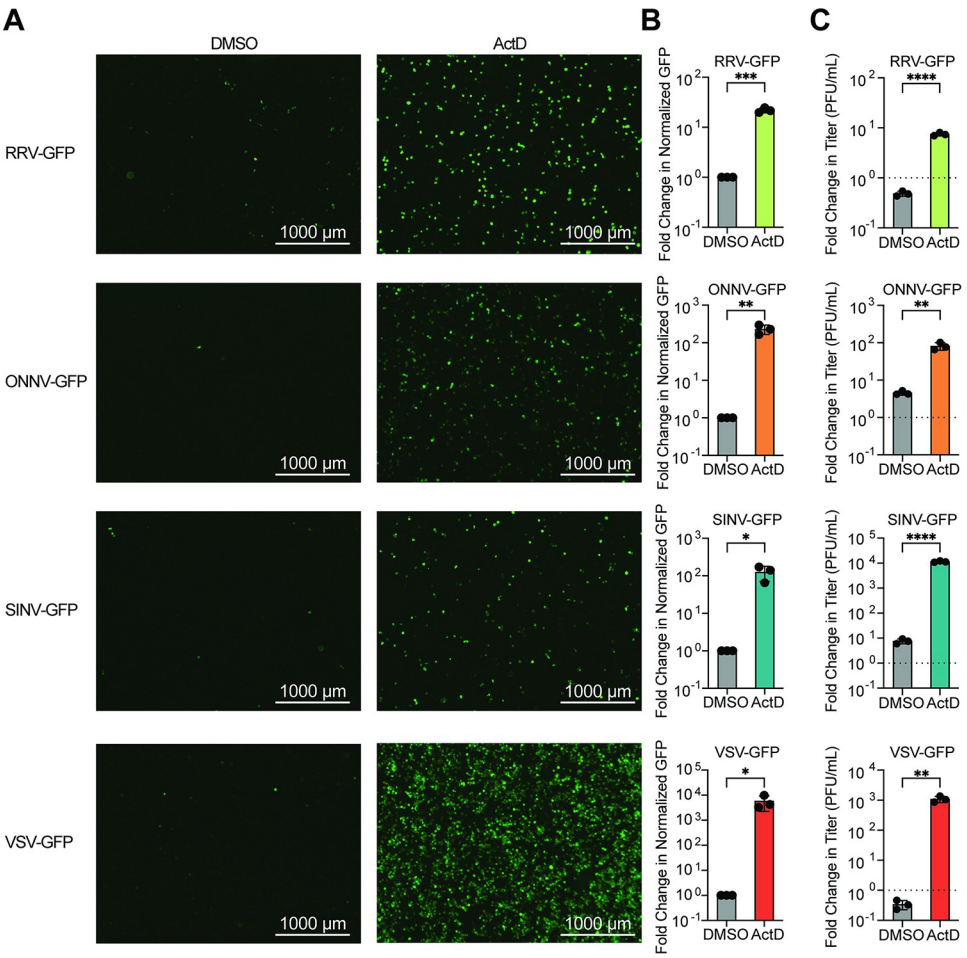

Fig 1. Abortive arbovirus replication in LD652 cells can be relieved with ActD treatment. A. Representative fluorescence microscopy images (GFP channel) of LD652 cells treated with DMSO (vehicle) or 0.05 μg/mL ActD and infected with the indicated GFP reporter strains for 72 h. **B.** Fold-change in normalized GFP signals in ActD-treated cultures relative to DMSO treatments. Cells were stained 72 hpi with CellTracker Orange dye (not shown) and imaged in GFP and RFP channels to calculate fold-change in GFP signal after normalization of cell number using CellTracker (RFP) channel signals. **C.** Fold-change in titer of supernatants from LD652 cell cultures treated as in **A**-**B** 72 hpi relative to input inoculum (dotted line). Data in B-C are means ± SD; n = 3. Statistical significance was determined with unpaired student's t-test; ns = P>0.1234, * = P<0.0332, ** = P<0.0021, *** = P<0.0002, **** = P<0.0001.

https://doi.org/10.1371/journal.ppat.1012010.g001

(control) plasmids. Effector proteins that enhanced viral GFP signals by >2.5-fold or luciferase signals by >4-fold above empty vector-transfected cells, were considered "hits" in our screen (Fig 2B–2E). These cutoffs were chosen to avoid false positives stemming from experimental noise within our screening system and allowed us to focus on effectors that robustly rescued arbovirus replication. Of the 210 effector proteins screened, 10 effectors rescued RRV-GFP, 11 rescued ONNV-GFP, 18 rescued SINV-LUC, and 10 rescued VSV-LUC (Fig 2B–2F and S1 Table). Interestingly, effectors generally rescued in a virus-specific manner. For instance, 21 effectors only rescued one of the four arboviruses screened (Fig 2F). This suggests that these effectors may relieve virus-specific restrictions to replication. In contrast, seven effectors rescued three or more arboviruses: IpaH4, SopB, HopT1-2, HopAM1, Ceg10, EspK, and SidM (Fig 2F), suggesting that these effectors may target host restriction mechanisms that are active against a broader range of viral pathogens. Importantly, we also assessed LD652 cells for signs of toxicity due to effector expression using a lactate dehydrogenase (LDH)-based cytotoxicity

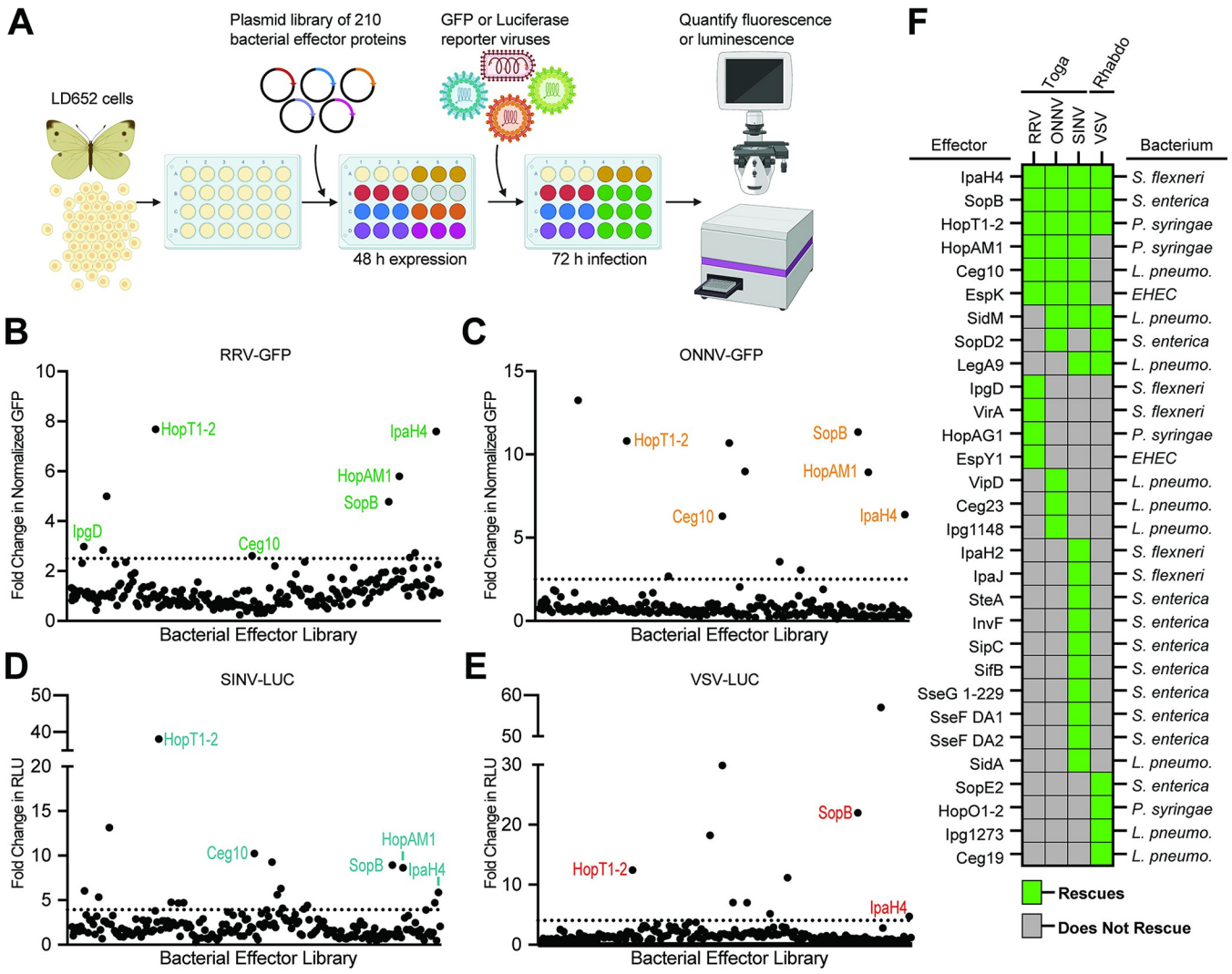

Fig 2. Specific Bacterial Effectors Relieve Arbovirus Restriction in LD652 Cells. A. Schematic outlining screen for bacterial effectors that rescue arbovirus restriction in LD652 cells. Cells were transfected with expression plasmids from a library consisting of 210 different effector proteins. After 48 h, cells were infected with either GFP or luciferase reporter strains. At 72 hpi, viral replication was quantified using fluorescence microscopy (RRV-GFP and ONNV-GFP) or luciferase assays (VSV-LUC and SINV-LUC). Image was created with BioRender.com. **B-E.** Fold-change in reporter readout, normalized to empty vector controls for all four screens. The cutoff for fold-change in GFP-based assays was set to >2.5, while the cutoff for luciferase reporters was set to >4-fold (represented by dotted horizontal lines). Data points are means. RLU = relative light units. **F.** Summary of bacterial effector proteins that rescued at least one virus. Green blocks indicate the effector rescued the virus indicated in the column header. The bacterium encoding each effector is noted to the right: *Shigella flexneri* (*S. flexneri*), *Pseudomonas syringae* (*P. syringae*), *Salmonella enterica* (*S. enterica*), *Legionella pneumophila* (*L. pneumo.*) *Enterohemorrhagic Escherichia coli* 0157:H7 (EHEC). Additional effector proteins from *Yersinia pseudotuberculosis* and *Bartonella henselae* were also screened but did not rescue arbovirus replication. The complete list of effectors screened and the raw results of the screens can be found in **S1 Table**.

https://doi.org/10.1371/journal.ppat.1012010.g002

assay (**S1A–S1C Fig and S1 Table**). Overall LDH activity in effector-transfected cultures was within 13–14% of that measured in empty vector-transfected cells, indicating that effector expression had minimal impact on cell viability. This suggests that enhanced arbovirus replication observed in effector treatments was unlikely due to generalized effects on cell viability.

Diverse effector activities are required for viral rescue

Because our original effector library did not encode epitope-tagged effector genes, we wanted to confirm the expression and rescue functions of key hits from our screen. To do this, we

chose five effectors: SopB, HopT1-2, HopAM1, Ceg10, and IpaH4 that rescued at least 75% of the arboviruses screened. Although EspK and SidM effectors also rescued 75% of the arboviruses screened, we did not pursue these effectors further as we wanted to keep our analysis to a manageable number and these effectors will be the subject of future investigations. The five effectors we chose to further analyze are collectively encoded by four bacterial pathogens and have distinct known or putative structures and functions (**Fig 3A**). In addition to these, we included IpgD in our downstream analysis due to the homology it shares with one of the top hits, SopB (discussed below). We cloned these six effectors into a novel expression vector, pDGOpIE2, along with Flag epitope tags (**Fig 3B**). The pDGOpIE2 vector uses the same baculovirus-derived OpIE2 promoter [24] to drive effector expression as in the pIB/V5-His vector used in our initial screen, but the former vector encodes unique restriction sites that facilitated restriction enzyme-based cloning (**S2 Fig**). Using these constructs, we confirmed the expression of all six Flag-tagged effectors by immunoblot in LD652 cells. We also confirmed the expression of specific point mutants in some of these effectors (described below) predicted to inactivate effector enzymatic activities (**Fig 3B**). Importantly, these pDGOpIE2-based effector constructs did not affect LD652 cell viability relative to empty pDGOpIE2 vector control treatments (**S3 Fig**). We next transfected either wild-type or mutant effector expression constructs into LD652 cells to determine: 1) if these Flag-tagged effectors could rescue arbovirus replication and 2) if known or putative enzymatic functions were required for viral rescue. Below we discuss each of these effectors and their ability to rescue restricted arbovirus replication.

SopB is encoded by *Salmonella enterica* serovar Typhimurium and functions as a phosphatase to generate phosphatidylinositol-5-phosphate (PI(5)P) from PI(4,5)P to activate Phosphoinositide 3-kinase (PI3K) signaling [25]. This activity has been shown to promote bacterial entry by inducing membrane ruffling [26] as well as altering endosomal maturation and trafficking [27]. The phosphatase activity of SopB relies on a catalytic cysteine (C420) [25] and mutants encoding a C420S substitution ($SopB^{C420S}$) have impaired enzymatic activity [28,29]. When expressed in LD652 cells, we found that wild-type SopB significantly enhanced the replication of all four arboviruses, while $SopB^{C420S}$ did not significantly affect arbovirus replication when compared to empty vector control treatments (**Fig 3C–3F**). Importantly, this lack of rescue by the $SopB^{C420S}$ mutant was not due to poor expression as it expressed to higher levels than wild-type SopB (**Fig 3B**). Interestingly, the degree of arbovirus rescue was variable among the viruses assayed. For instance, while SopB enhanced RRV-GFP by only ~three-fold over empty vector controls, it increased the other three viruses by ~30-80-fold. Although the absolute fold changes in arbovirus replication varied between our initial screen using pIB/V5-His and our confirmatory screen with pDGOpIE2, the overall trends in SopB rescue were similar (**Fig 2B–2E** versus **Fig 3C–3F**). Interestingly, the *Shigella flexneri*-encoded IpgD effector shares ~47% amino acid identity to SopB and can also generate (PI(5)P) from PI(4,5)P reliant on a conserved catalytic cysteine (C439) [30,31]. Therefore, it was surprising that IpgD only rescued one arbovirus in our initial screens. However, several immunoblot experiments failed to detect Flag-tagged IpgD expression in LD652 cells when cloned into pDGOpIE2, suggesting that IpgD may express more poorly in insect cells than SopB. Thus, we cloned a codon-optimized, Flag-tagged form of IpgD into pDGOpIE2 vectors and re-tested its ability to rescue all four arboviruses. Strikingly, we found the codon-optimized IpgD expressed in immunoblots (**Fig 3B**) and enhanced the replication of all four arboviruses (**Fig 3C–3F**). This illustrates that poor expression of some effectors in our library may have produced false negatives. Importantly, expression of a catalytically-inactive mutant $IpgD^{C439S}$ [32] failed to rescue arbovirus replication, despite robust expression (**Fig 3B–3F**). These data suggest that a common phosphatase activity encoded by effectors from *S. enterica* and *S. flexneri* can break arbovirus restriction in LD652 cells.

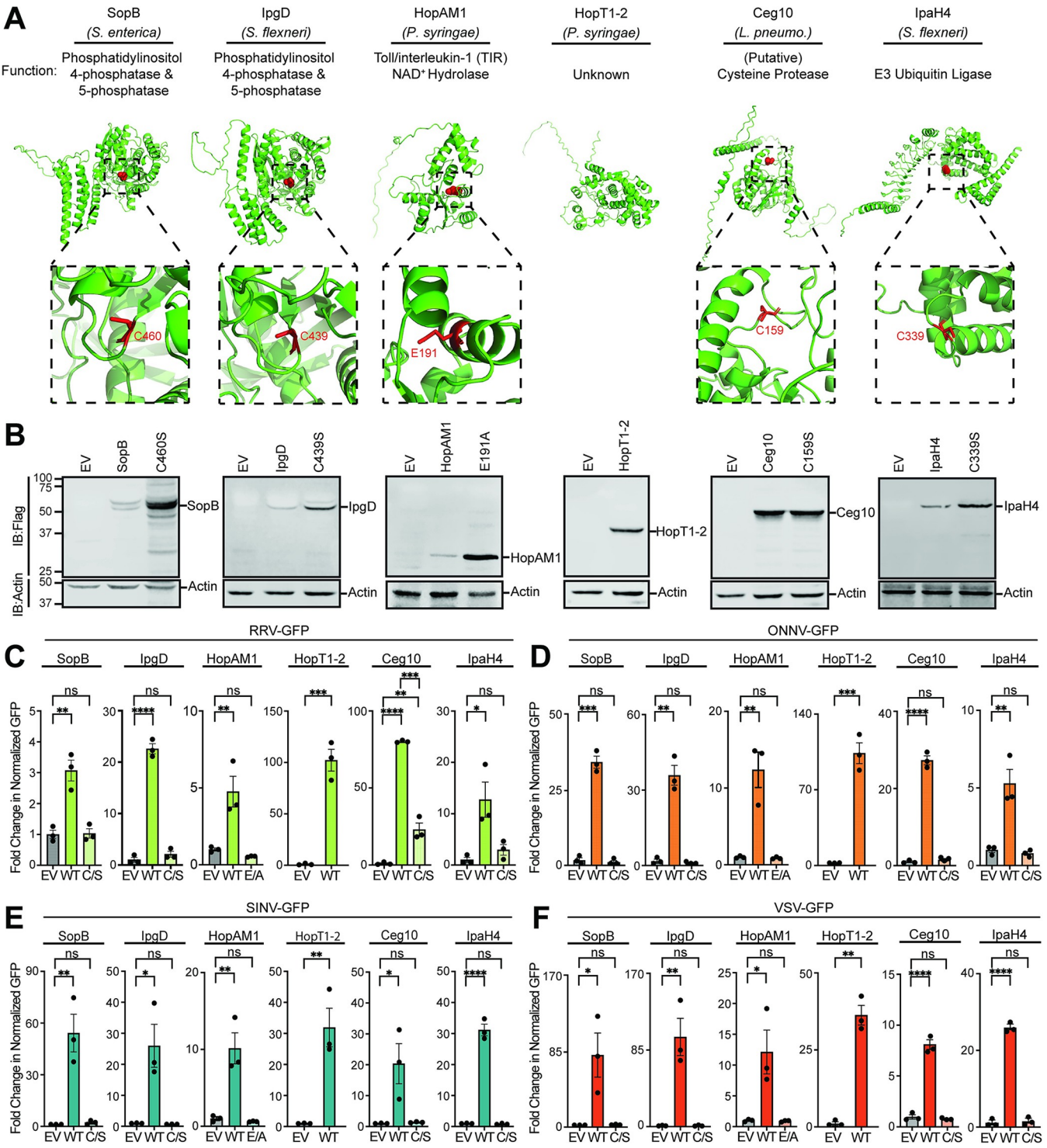

Fig 3. Validation and characterization of top hits from bacterial effector screens. A. AlphaFold predicted structures, and known or predicted enzymatic functions for indicated effector proteins identified as hits in arbovirus screens. Effector catalytic residues where substitution mutations were made are highlighted in red in AlphaFold structures. **B.** Representative immunoblots of Flag-tagged bacterial effector expression in LD652 cells 48 h post transfection. **C-F.** Fold-change in normalized viral GFP signal relative to empty vector (EV) controls 72 hpi with after transfection with indicated Flag-tagged effector constructs. Wild-type (WT) effectors are compared to their mutants (E/A or C/S). Cells were stained 72 hpi with CellTracker dye and imaged to calculate fold-change in normalized GFP signal over signals in EV treatments. Data in C-F are means ± SD; n = 3. Statistical significance was determined with unpaired student's t-test; ns = P>0.1234, * = P<0.0332, ** = P<0.0021, *** = P<0.0002, **** = P<0.0001.

https://doi.org/10.1371/journal.ppat.1012010.g003

The effector gene library used to screen for viral rescue included effectors encoded by the plant pathogen *Pseudomonas syringae*. It was therefore notable that two effectors, HopAM1 and HopT1-2, rescued arbovirus replication within the insect cells. These data suggest that host substrates of effectors, highly conserved through to *Plantae*, can reveal novel points of viral restriction. The HopAM1 effector possesses a toll-like receptors and interleukin-1 receptors (TIR) domain that suppresses pattern-triggered immunity in plant hosts [33]. HopAM1 was recently shown to catalyze the formation of a novel cyclic adenosine monophosphate (ADP)-ribose (cADPR) isomer, termed "v2-cADPR" [33], which is required for its immunosuppressive function and for *P. syringae* pathogenicity [34]. The hydrolase activity of HopAM1 requires a catalytic glutamate (E191) to hydrolyze nicotinamide adenine dinucleotide (NAD^+) into v2-cADPR [33]. Expression of Flag-tagged HopAM1 constructs in LD652 cells significantly enhanced the replication of all four arboviruses, while a catalytically-inactive mutant ($HopAM1^{E191A}$) [35] did not significantly affect arbovirus replication (**Fig 3B–3F**). HopT1-2 has also been implicated in suppressing plant immunity. Previous work has demonstrated that HopT1-2 antagonizes "nonhost resistance" defenses in plants [36] by suppressing expression of nonhost 1 proteins required for this immune response [37]. However, the molecular mechanism underlying this HopT1-2 function remains unknown. AlphaFold predicted structures (**Fig 3A**) and Hhpred homology determination software [38] were unable to identify a putative catalytic activity for HopT1-2. Expression of Flag-tagged HopT1-2 was confirmed by immunoblot in LD652 cells and this construct rescued all four restricted arboviruses as we observed in our original screen (**Fig 3B–3F**). Together, these results illustrate that two specific effectors encoded by a plant pathogen can antagonize antiviral responses in animal cells. Future studies will be needed to determine how the generation of v2-cADPR or the resulting NAD^+ depletion breaks viral restriction, as well as the functional role of HopT1-2 during infection.

In addition to identifying effector proteins with known host substrates, our unbiased screen uncovered novel effector proteins involved in breaking host immunity. Ceg10 is an uncharacterized effector secreted by *Legionella pneumophila*, the causative agent of human Legionnaires' disease [39]. BLAST homology searches identified proteins closely related to Ceg10 in different *Legionella* serovars, yet sequence comparisons did not reveal a putative function. We therefore took a structural biology approach to help assign a function to Ceg10. We were unable to obtain crystals suitable for X-ray crystallography with full-length Ceg10, possibly owing to flexible N- and C-terminal domains as determined by the AlphaFold prediction (**Fig 3A**). We then used limited proteolysis to produce a core Ceg10 central domain (T55-R287) that was amenable to structural determination by crystallography (**Fig 4A**). We determined the structure of the trypsin limited-proteolysis protected core ($Ceg10^{TR}$) from three different data sets to 1.7 Å, 1.4 Å and 1.5 Å resolution, respectively (**S2 Table**).

Overall, $Ceg10^{TR}$ is composed of 8 α-helices surrounding 7 β-sheets in a conformation resembling a cysteine proteinase with a putative catalytic triad consisting of Cys-159, His-196, and Asp-204 (**Fig 4A and 4B**). A structural search via the PDBeFold [40] reveals several homologs containing the Cys-His-Asp triad but with low sequence identity (**Fig 4A**). Interestingly, while the Cys-159 (C159) of Ceg10 is modeled in two roughly equal conformers in data set 1 (PDB ID: 9B8D), in data sets 2 and 3, C159 is modeled in only one conformer as a nitrosylated cysteine, or S-nitrosothiol [41] (PDB ID: 9B8E, **Fig 4B and 4C**). Despite this, both structural determinations overlap modestly (**Fig 4D**). All crystals used for data sets in this study were grown from the same batch of purified protein, but the crystallization condition for data set 1 was 2.0 M sodium, potassium phosphate whereas for data sets 2 and 3 the major precipitants were polyethylene glycols. The significant level of trace divalent metal ions present in commercial preparations of sodium or potassium phosphate, and the extended time between initiation of crystal growth and harvesting is likely the reason the protein crystallized in data set 1 has

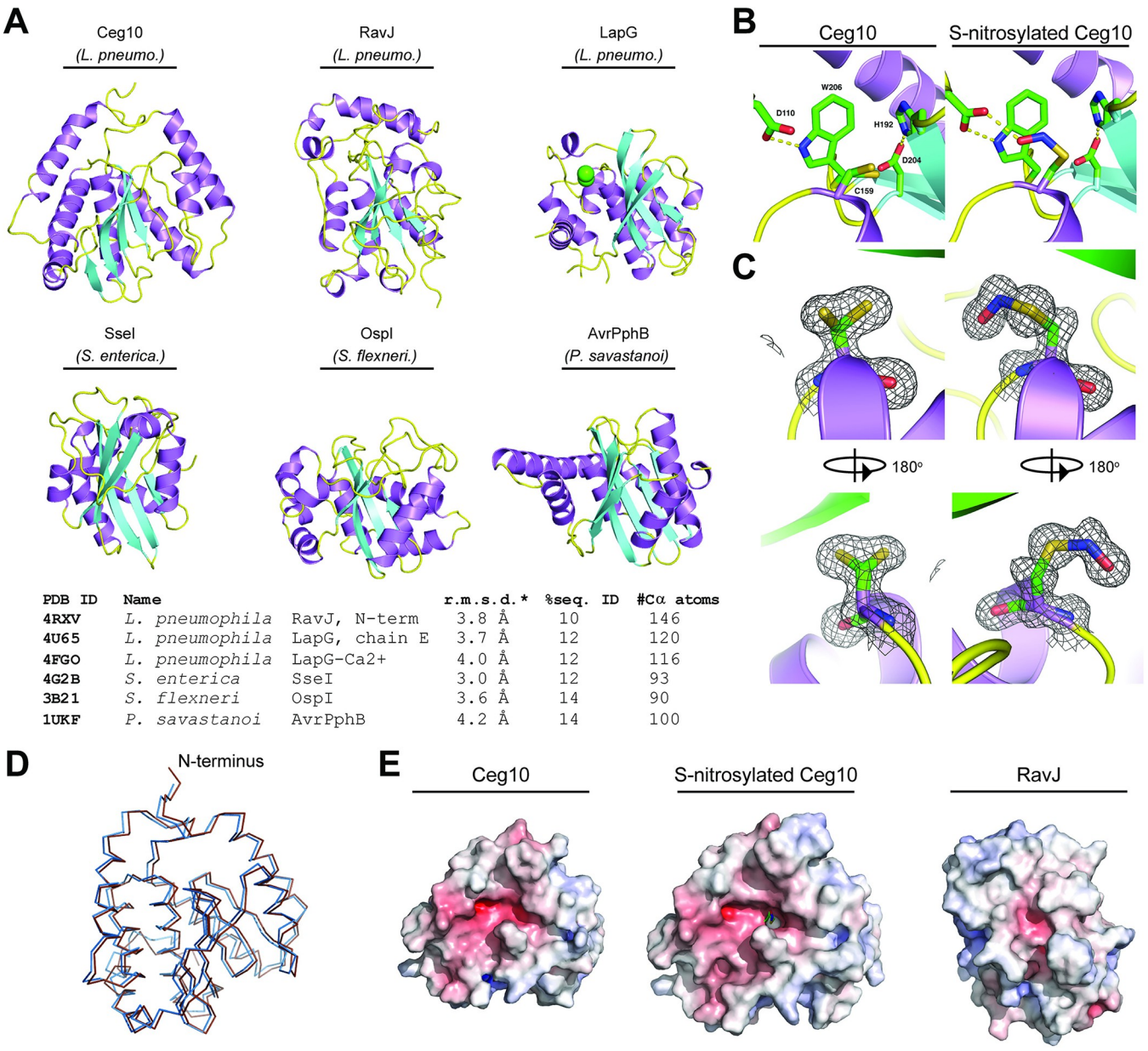

PDB ID	Name		r.m.s.d.*	%seq. ID	#Cα atoms
4RXV	*L. pneumophila*	RavJ, N-term	3.8 Å	10	146
4U65	*L. pneumophila*	LapG, chain E	3.7 Å	12	120
4FGO	*L. pneumophila*	LapG-Ca2+	4.0 Å	12	116
4G2B	*S. enterica*	SseI	3.0 Å	12	93
3B21	*S. flexneri*	OspI	3.6 Å	14	90
1UKF	*P. savastanoi*	AvrPphB	4.2 Å	14	100

Fig 4. Structural analysis of *Legionella pneumophila* effector Ceg10. A. Six structural homologs of Ceg10, shown in the same orientation with the putative active site near the top of the figure. Top row, from left: Ceg10 (this study), *L. pneumophila* RavJ, *L. pneumophila* LapG. Bottom row, from left: *S. enterica* SseI, *S. flexneri* OspI, *P. savastanoi* AvrPphB. Table shows these structural homologs as determined via the Dali Lite server and their PBD ID**. B.** The putative active site of Ceg10 with residues shown in stick representation and hydrogen bonds are shown as dotted yellow lines. The catalytic Cys (C159), Asp (D204) and His (H192) are labeled as well as residues Asp110 and Trp 206 which are hydrogen bonded to each other in both structures. In the S-nitrosylated structure, Asp110 also hydrogen bonds to the nitrosylated-C159 and van der Waals interactions occur between the aromatic ring of Trp206 and the nitrosylation moiety. **C.** Electron density for C159 in the native (left) and S-nitrosylated (right) Ceg10 structures. The final refined 2Fo-mDFc electron density map, contoured at the 1σ level, is shown superimposed on each residue, as well as a 180˚ rotation of this region. **C.** Superposition of native (blue) and S-nitrosylated (brown) Ceg10 structures. **D.** Electrostatic surface potential of both Ceg10 structures and RavJ. All structures are orientated with the putative catalytic cysteine residue in approximately the center of the surface, and the orientations between Ceg10 and RavJ correspond to protein alignments. The displayed surface is colored by electrostatic potential from -10 kT (red) to + 10 kT (blue), as calculated by the APBS plugin in PyMOL.

https://doi.org/10.1371/journal.ppat.1012010.g004

lost the S-nitrosothiol, as metal catalyzed decomposition has been well documented for this post-translational modification [42]. In the S-nitrosothiol structure, the carboxylate of Asp-110 is hydrogen bonded to both the nitrosyl oxygen of C159 and the sidechain of Trp-206 (**Fig 4B**).

The closest homolog of Ceg10, the *Legionella pneumophila* effector RavJ, is the only homolog that includes an analogous tryptophan (Trp-172) and aspartate (Asp-24), but the cysteine (Cys-101) is neither modified nor modeled in multiple conformations. Analysis of the electrostatic potential mapped to the surface of Ceg10 and RavJ reveals that the catalytic site of RavJ is buried while the S-nitrosothiol of Cys-159 in Ceg10 is solvent exposed (**Fig 4E**). These data together indicate that Ceg10 harbors a highly reactive catalytic cysteine that may be critical for regulating host responses to infection. Indeed, expression of Flag-tagged wild-type Ceg10 significantly enhanced the replication of all four arboviruses. Consistent with our structural analysis, conversion of the predicted catalytic cysteine to serine (C159S) generated a mutant ($Ceg10^{C159S}$) that was unable to rescue three of the four arboviruses screened, despite robust expression (**Fig 3B–3F**). Although $Ceg10^{C159S}$ significantly enhanced RRV-GFP replication compared to empty vector control, this rescue was significantly weaker than rescue observed with wild-type Ceg10 constructs (**Fig 3B–3F**). Further studies will be needed to confirm Ceg10 function and its regulation by S-nitrosylation, however, these data suggest that a putative cysteine protease encoded by *L. pneumophila* is capable of targeting antiviral immune pathways in insect cells.

Lastly, IpaH4 is secreted by *Shigella flexneri* which causes Shigellosis in humans [43]. IpaH proteins are a family of bacterial E3 ubiquitin ligases that consist of two domains: a leucine rich repeat domain (LRR) used for substrate specificity and a novel E3 ligase domain (NEL) containing the catalytic cysteine [15,44,45]. We confirmed expression of wild-type IpaH4 and demonstrated significant viral rescue in all cases, however, an IpaH4 mutant with a serine substitution at position 339 ($IpaH4^{C339S}$) was unable to rescue any arbovirus tested (**Fig 3B–3F**). Our group [46–48] and others [49,50] have shown that IpaH proteins antagonize various eukaryotic immune response pathways by targeting host defense proteins for degradation. However, IpaH4 has remained an uncharacterized member of the IpaH family. Thus, we were interested in both determining if IpaH4 was indeed an active E3 ubiquitin ligase and uncovering the putative host substrates that it targets.

IpaH4 is an E3 ubiquitin Ligase that directly targets host PSMC1 and SHOC2 proteins

To confirm that IpaH4 exhibits E3 ubiquitin ligase activity, we performed *in vitro* autoubiquitination assays. E3 ubiquitin ligase activity can be revealed by demonstrating: 1) autoubiquitination function; 2) polymerization of free ubiquitin chains; and/or 3) direct ubiquitination of a substrate [51,52]. Given that the substrates of IpaH4 are unknown, we conducted *in vitro* autoubiquitination experiments with GST-tagged IpaH4 (GST-IpaH4) purified from *E. coli*. Ubiquitination is a post-translation modification that transfers ubiquitin molecules from E1 (ubiquitin-activating enzymes) to E2 (ubiquitin-conjugating enzymes) to E3 ubiquitin ligases, which ultimately covalently attach ubiquitin to target proteins [53]. When mixed with the necessary components of a ubiquitination reaction: E1, E2, ubiquitin, and ATP, GST-IpaH4 displayed clear autoubiquitination as evidenced by the formation of higher molecular weight species that reacted with anti-GST and anti-ubiquitin antibodies (**Fig 5A**). However, when E1 was removed from these *in vitro* reactions, these higher molecular weight species were not detected, as expected (**Fig 5A**). Interestingly, under these reaction conditions, we were unable to observe autoubiquitination activity for two additional IpaH family members, IpaH2.5 and

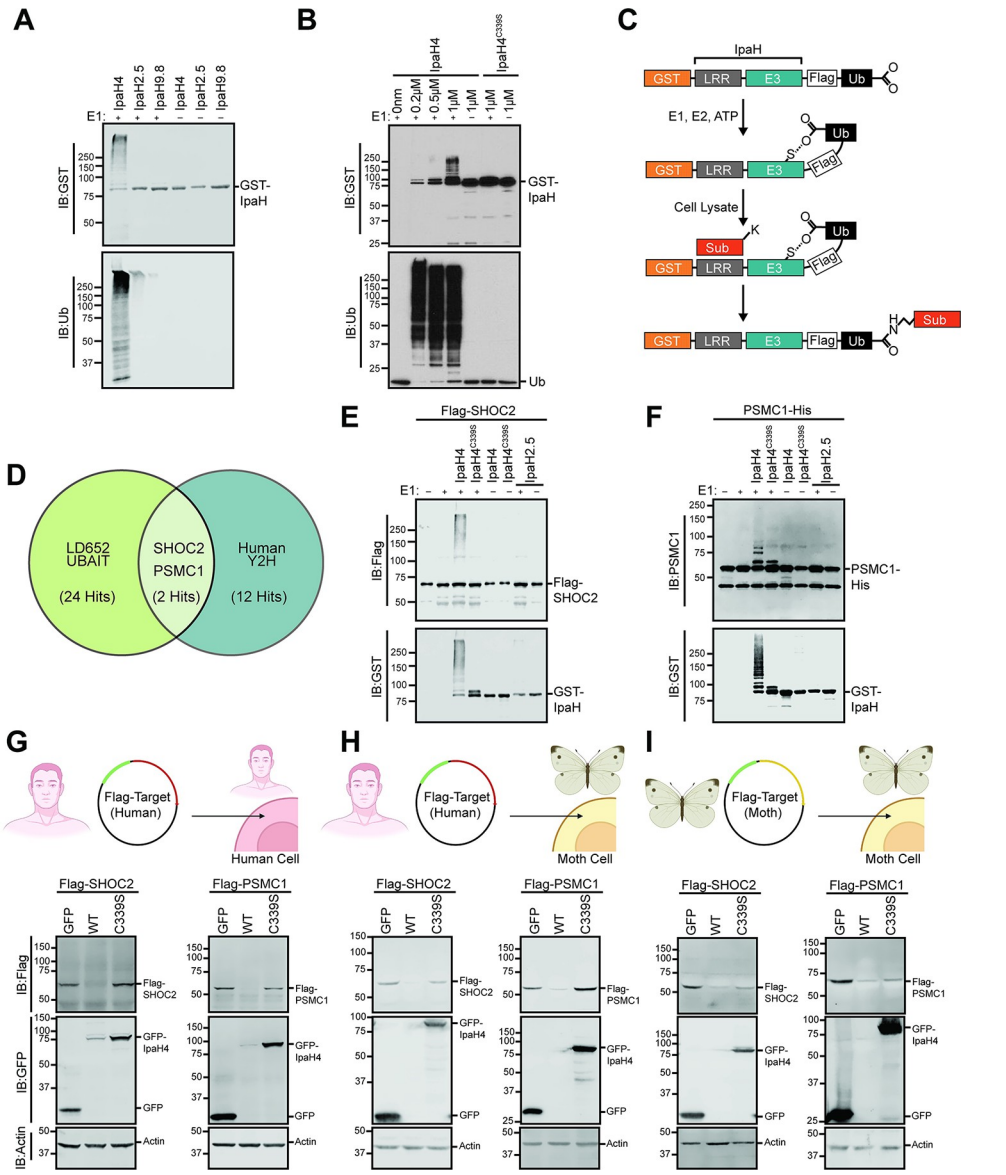

Fig 5. Identification of host SHOC2 and PSMC1 as conserved targets of IpaH4. A. Representative immunoblot of *in vitro* ubiquitination assay performed with indicated GST-IpaH proteins in the absence of substrates. **B.** Representative immunoblot of *in vitro* ubiquitination assay performed with indicated concentrations of wild-type GST-IpaH4 or GST-IpaH4^{C339S} mutant proteins. **C.** Schematic outlining UBAIT protocol [53,56]. **D.** Venn diagram showing conserved putative substrates (overlapping region) of IpaH4 across UBAIT experiments (n = 3) in LD652 cell lysates and Y2H screens (n = 2) against a human prey library. **E.** Representative immunoblot of *in vitro* ubiquitination assay showing IpaH4-mediated ubiquitination of human Flag-SHOC2 proteins. **F.** Representative immunoblot of *in vitro* ubiquitination assay showing IpaH4-mediated ubiquitination of human PSMC1-His proteins. **G.** Representative immunoblot of degradation assays using indicated Flag-tagged human proteins in transfected HEK293T cells co-expressing GFP, IpaH4 (WT) or catalytic mutant GFP-IpaH4^{C339S} (C339S). **H.** Representative immunoblot of degradation assays using indicated Flag-tagged human proteins in transfected LD652 cells co-expressing GFP, IpaH4 (WT) or catalytic mutant GFP-IpaH4^{C339S} (C339S). **I.** Representative immunoblot of degradation assays of Flag-tagged moth (*L. dispar*) protein in LD652 cells expressing GFP, IpaH4 (WT) or catalytic mutant GFP-IpaH4^{C339S} (C339S). Images in **G-I** were created with BioRender.com.

https://doi.org/10.1371/journal.ppat.1012010.g005

IpaH9.8 (Fig 5A). This finding is consistent with prior observations that IpaH members typically display autoinhibition unless in the presence of substrates [54,55]. Thus, the robust IpaH4 autoubiquitination observed in the absence of substrates suggests an important distinction of IpaH4 autoregulation when compared with other IpaH members, and may contribute to the lower wild-type IpaH4 expression observed in cellular assays (e.g. **Fig 3B**) as it may be efficiently turned over by the proteasome. GST-IpaH4 autoubiquitination activity could be detected at wide range of protein concentrations (0.2–1 μM) and typically became more obvious at higher IpaH concentrations. However, the GST-IpaH4^{C339S} mutant predicted to inactivate the catalytic cysteine, was unable to display detectable autoubiquitination even at 1 μM concentrations (**Fig 5B**).

Next, we sought to identify the host substrates of IpaH4. As IpaH4 is encoded by a human pathogen and was able to rescue arbovirus replication in insect cells, we hypothesized that the natural substrates of IpaH4 may be highly conserved between mammals and invertebrates. Therefore, we employed two distinct approaches to identify putative targets of IpaH4 in both moth and human backgrounds. First, ubiquitin activated interaction trap (UBAIT) assays [53,56] were conducted in LD652 whole cell extract (**Fig 5C**). We have used this approach previously to identify the host substrates of other IpaH members [46,47]. Briefly, the human ubiquitin gene was cloned in frame with IpaH4 to generate a C-terminal fusion protein (IpaH4^{UBAIT}). This fusion allows IpaH proteins to bind their substrates through their N-terminal LRR domains and catalyze thiol-mediated ligation of the fused ubiquitin to a lysine on their substrates [56]. This results in the covalent linkage of IpaH proteins to their substrates, allowing their identification by mass spectrometry after affinity purification of IpaH-substrate complexes [56]. Using this approach, we identified 24 moth proteins that were enriched at least five-fold in IpaH4^{UBAIT} reactions compared to UBAIT reactions conducted with IpaH2.5^{UBAIT} constructs, which served as our control (**Fig 5D and S3 Table**).

Because our goal was to identify evolutionarily conserved mechanisms of host immunity, we took advantage of an existing commercial human prey library and conducted two independent yeast two-hybrid (Y2H) screens using IpaH4 bait. An advantage of using a Y2H approach is that we can identify direct IpaH4-substrate interactions whereas UBAIT techniques tend to identify both direct and indirect IpaH-host interactions. Furthermore, by comparing the putative host substrates identified with UBAIT in the moth system with putative targets identified in human Y2H prey screens, we can detect substrate interactions common between two distinct approaches, and thus more likely to be bona fide interactors. Our Y2H screens with IpaH4 bait identified 12 human proteins as putative IpaH4 interactors with >2 independent clones identified across two screens (**Figs 5D and S4A, and S3 Table**). We then compared both UBAIT and Y2H screening results and found Leucine-rich repeat protein SHOC2 and proteasome 26S subunit, ATPase 1 (PSMC1; also known as Rpt2) to be the only two reproducibly identified putative substrates across moth and human backgrounds (**S4A Fig**).

To determine if IpaH4 directly ubiquitinates purified human SHOC2 or PSMC1 proteins, *in vitro* ubiquitination assays were conducted. Recombinant Flag-SHOC2 or PSMC1-His proteins were incubated with GST-IpaH4, E1, E2, ubiquitin, and ATP as described above for our autoubiquitination assays. Wild-type GST-IpaH4, but not GST-IpaH4^{C339S}, was capable of ubiquitinating both host proteins in an E1-dependent manner, as evidenced by the formation of higher molecular weight Flag-SHOC2 and PSMC1-His species (**Fig 5E and 5F**). In contrast, incubation with GST-IpaH2.5 did not result in ubiquitination of either protein (**Fig 5E and 5F**). These results suggest that IpaH4 specifically ubiquitinates both SHOC2 and PSMC1 *in vitro*.

Next, given that other IpaH family members ubiquitinate substrates for proteasomal degradation [47,49,50], we hypothesized that intracellular SHOC2 and PSMC1 protein levels may

be reduced in the presence of IpaH4. To assess this, degradation assays were conducted by co-expressing GFP-tagged IpaH4 with Flag-tagged human or moth SHOC2 and PSMC1 constructs in order to determine if IpaH4 activity altered intracellular levels of these putative substrates. Both human Flag-SHOC2 and Flag-PSMC1 levels were dramatically reduced when co-transfected with wild-type GFP-IpaH4 constructs, when compared to co-transfections with GFP- or GFP-IpaH4^{C339S}-expressing vectors in HEK293T cells (**Fig 5G**). Other putative targets of IpaH4 (**S4A Fig**) such as SLU7, PRPF6, CRTC1, and BRD7 that were identified in our Y2H screen with human prey but not in our moth UBAIT assays, mostly showed little-to-no reduction in their levels in HEK293T cells when in the presence of GFP-IpaH4 (**S4B Fig**). One exception to this trend was human RNF214, which was dramatically reduced in level when co-expressed with GFP-IpaH4 (**S4B Fig**). However, RNF214 lacks a discernable *L. dispar* ortholog [14] and therefore was unlikely to be involved in arbovirus restriction in LD652 cells.

We next sought to determine if SHOC2 and PSMC1 were targeted by IpaH4 in the insect cell background. We found that human Flag-SHOC2 and Flag-PSMC1 proteins were dramatically reduced in abundance when co-transfected with GFP-IpaH4 in LD652 cells, suggesting that IpaH4 can target these human proteins when expressed in either human or moth cells (**Fig 5H**). To determine if IpaH4 can also alter the levels of moth-encoded SHOC2 and PSMC1 proteins, we co-transfected Flag-tagged versions of these putative moth targets into LD652 cells in the absence or presence of GFP-IpaH4. These experiments demonstrated that GFP-IpaH4, but not GFP-IpaH4^{C339S} constructs, could dramatically reduce moth Flag-SHOC2 and Flag-PSMC1 levels (**Fig 5I**). Collectively, these results suggest that wild-type, but not catalytically-inactive IpaH4 proteins, can reduce the levels of SHOC2 and PSMC1 proteins encoded by both *L. dispar* and human hosts.

Depletion of SHOC2 and PSMC1 rescues restrictive arbovirus replication in LD652 cells

One prediction of our approach is that the host substrates of effector proteins secreted by mammalian and plant pathogens are key regulators of viral restriction in the moth. To then determine if endogenous SHOC2 proteins contributed to arbovirus restriction in moth cells as our data suggests, we adapted a previously described CRISPR-Cas9 system for disrupting gene expression in lepidopteran insects [57] to inhibit SHOC2 expression. We cloned two independent single-guide RNAs (sgRNAs) targeting *L. dispar SHOC2* into pIE1-Cas9-SfU6-sgRNA-Puro [57], an "all-in-one" vector system that expresses Cas9 nuclease, sgRNA, and a puromycin resistance cassette for selection. As controls, cells were transfected with either empty vector or a sgRNA targeting the *L. dispar relish* gene, which encodes a Nuclear Factor-κB-like transcription factor that we have shown to contribute to VSV and SINV restriction in LD652 cells [12,22]. Transfected cells underwent three rounds of puromycin selection and were then challenged with reporter arboviruses. As expected, cells expressing sgRNA targeting *relish* were significantly more susceptible to VSV-GFP and SINV-GFP infection when compared to empty vector control treatments. RRV-GFP and ONNV-GFP replication was also elevated in cells expressing *relish*-targeted sgRNAs, indicating that these togaviruses are also restricted by Relish-dependent antiviral responses (**Fig 6A**). Interestingly, cells expressing either *SHOC2* sgRNA-A or sgRNA-B were significantly more susceptible to infection with ONNV-GFP, SINV-GFP, and VSV-GFP infection (**Fig 6A**). While only cells expressing *SHOC2* sgRNA-A displayed statistically-significant differences in RRV-GFP infection, *SHOC2* sgRNA-B-expressing cells trended towards an increased susceptibility to this virus with an ~9-fold higher mean in GFP signal than empty vector controls (**Fig 6A**). We then sought to assess if viral titers were also enhanced after arbovirus infection in SHOC2 sgRNA-expressing cells. Thus, we

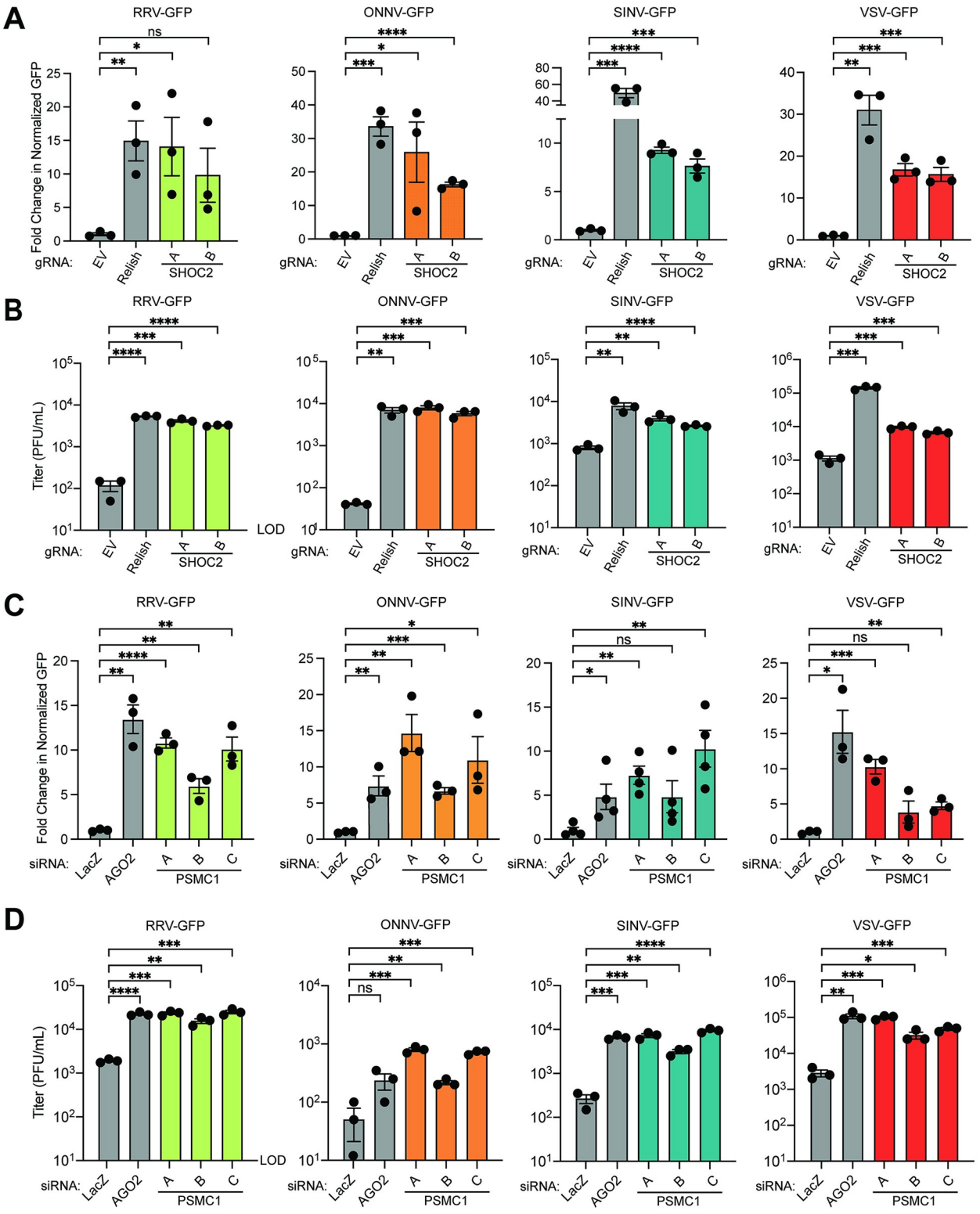

Fig 6. Depletion of IpaH4 substrates SHOC2 and PSMC1 enhances arbovirus replication in LD652 cells. A. Fold-change in normalized viral GFP signals in cells expressing gRNA targeting Relish or SHOC2 relative to empty vector controls 72 hpi. Cells were stained with CellTracker dye 72 hpi and imaged to calculate fold-change in normalized GFP signal over empty vector (control) treatments. Data are means ± SD; n = 3. Statistical significance was determined with unpaired student's t-test. **B.** Titer of supernatants from LD652 cell cultures treated as described in **A**. **C.** Fold-change in normalized viral GFP signals relative to LacZ siRNA (control) treatments. Cells were stained with CellTracker dye 72 hpi and

imaged to calculate fold-change in normalized GFP signal over LacZ (control) siRNA treatments. **D.** Titer of supernatants from LD652 cell cultures treated as described in **C**. Data are means ± SD; n = 3. Statistical significance was determined with unpaired student's t-test; ns = P>0.1234, * = P<0.0332, ** = P<0.0021, *** = P<0.0002, **** = P<0.0001.

https://doi.org/10.1371/journal.ppat.1012010.g006

repeated these infections and collected the supernatants following 72 h of infection before determining viral titers on BSC-40 cells. Overall, the trends observed in **Fig 6A** with increases in GFP signal in SHOC2 sgRNA-expressing cells correlated well with increases in viral titers across the four arboviruses (**Fig 6B**), although the magnitude of the increases sometimes differed between fluorescence and titer-based experiments, which likely reflects differences in the nature of the readout of these assays. These results indicate that SHOC2 is a broadly-acting restriction factor for multiple arboviruses in LD652 cells. However, the specific role of SHOC2 in arbovirus restriction requires further investigation.

PSMC1 has been reported to be an essential component of the 19S cap of the 26S proteasome [58]. Consistent with this, our attempts to knock out PSMC1 in LD652 cells with CRISPR-Cas9 techniques resulted in complete cell death after 1–2 rounds of puromycin selection. However, in mammalian systems, transient PSMC1 depletion has been achieved by siRNA knockdown [59]. Therefore, we sought to deplete PSMC1 in LD652 cells in an analogous manner. However, the application of siRNA-based RNAi in *L. dispar* and other lepidopteran cell types has not been well-established. Thus, we took advantage of a prior study that developed guidelines for designing siRNAs to achieve efficient knockdown in another moth species, *Bombyx mori*, as a basis for our siRNA design for use in LD652 cells [60]. To evaluate the efficiency of siRNA-mediated RNAi in LD652 cells, we designed siRNA targeting the coding sequences of *E. coli LacZ* (negative control) and firefly luciferase. Cells were transfected with either an empty vector or a luciferase-encoding pDGOpIE2 plasmid for 48 h and then subsequently transfected with siRNAs targeting transcripts encoding LacZ or luciferase (**S5A Fig**). We then evaluated the relative expression of luciferase using luminescence assays 72 h later. Compared to luciferase signals observed in cells transfected with control LacZ siRNA, there was a significant ~75% reduction in luminescence signals in cells transfected with siRNA targeting transcripts encoding luciferase (**S5B Fig**), suggesting our siRNA design and transfection strategy was relatively efficient at reducing target gene expression.

We next designed three independent siRNAs targeting *L. dispar PSMC1* sequence in LD652 cells [14] and assessed their relative impact on PSMC1 levels compared to treatments where control siRNAs targeting LacZ were transfected. As a positive control for arbovirus rescue, siRNAs targeting transcripts encoding argonaute-2 (AGO2), which we have shown to restrict VSV and SINV replication in LD652 cells [61], were also transfected into cells. Compared to LacZ (negative control) siRNA treatments, at least 2/3 *PSMC1*-targeting siRNA transfections resulted in significant increases in viral GFP signals for all four arboviruses (**Fig 6C**). Importantly, we confirmed knockdown of PSMC1 in LD652 cells and found that *PSMC1* siRNAs-A and -C were the most effective at reducing protein level (**S5C Fig**), which correlated with viral rescue phenotypes (**Fig 6C**). Following these observations, we repeated these knockdown experiments to determine impacts on viral titers. Again, the overall trends we observed in **Fig 6C** with increased GFP signals in PSMC1 depletion conditions correlated well with increases in viral titers across the four arboviruses (**Fig 6D**). These data indicate that, like SHOC2, PSMC1 may also play a role in restricting arbovirus replication in LD652 cells. Given that PSMC1 is a proteasome subunit, we asked if treatment of LD652 cells with the proteasome inhibitor bortezomib (Bort) would alter their susceptibility to arbovirus infection. Interestingly, addition of Bort to cell culture media 2 hpi resulted in significantly greater viral replication by 72 hpi (**S6A and S6B Fig**). These data suggest that depletion of a proteasome subunit

or inhibition of proteasome activity sensitizes LD652 cells to arbovirus infection. However, the mechanism(s) by which PSMC1 and proteasome activity restrict arbovirus replication will require additional studies in the future.

IpaH4 activity or SHOC2/PSMC1 depletion breaks the restriction of oncolytic virus replication in refractory human cancer cells

After using IpaH4 as a molecular tool to uncover roles for SHOC2 and PSMC1 in viral restriction in insect hosts, we next wanted to examine if these host factors have conserved antiviral roles in mammalian hosts. However, the wild-type arboviruses used in our study are already well-adapted for robust replication in mammalian host cells. Therefore, we sought an alternative approach to examine whether SHOC2 and PSMC1 contribute to virus restriction in mammals.

Oncolytic virotherapy involves the use of viruses to replicate in, and destroy, cancerous cells. These viruses can also invoke anti-tumoral adaptive responses *in vivo*. For example, VSV strains encoding a deletion or arginine substitution of methionine 51 in the VSV matrix (M) protein (VSVΔM51/M51R) are being intensively pursued as a potential oncolytic agent [62–67]. These strains display a relatively safe profile because their mutant M proteins are unable to block cellular gene expression and thus are highly susceptible to innate immune responses (e.g. IFN signaling) that are present in normal cells, but typically defective in transformed cells [62–67]. However, a wide array of human cancer cell lines and tumor types have been shown to be refractory to VSVΔM51/M51R replication, presumably due restriction pathways that are still active in transformed cells [68–72]. This barrier to oncolytic VSV strain replication in refractory cancer types poses a significant challenge to the broad use of these strains for treating diverse malignancies [69,73]. Given that IpaH4 expression could break wild-type VSV restriction in LD652 cells, we asked whether this bacterial effector could also break restriction of a VSV-M51R strain encoding GFP (VSV-M51R-GFP) in refractory 786–0 human adenocarcinoma cells [70,74]. Interestingly, transfection of Flag-IpaH4 expression constructs into 786–0 cells led to a significant increase in VSV-M51R-GFP replication compared to empty vector (control) treatments. In contrast, Flag-IpaH4^{C339S} expression did not rescue VSV-M51R-GFP replication, indicating that IpaH4 E3 ubiquitin ligase activity was required to enhance the susceptibility of 786–0 cells to viral replication (**Fig 7A and 7B**). These results also demonstrate that, as in moth cells, IpaH4 can sensitize human cells to VSV infection and demonstrate that bacterial effectors may be useful tools for breaking oncolytic virus restrictions in refractory human cancer cells.

Finally, we asked whether the targets of IpaH4 we identified (SHOC2 and PSMC1) may contribute to virus restriction in human 786–0 cells as observed in moth LD652 cells. To assess the impact of human SHOC2 and PSMC1 on VSV-M51R-GFP restriction, we used three independent siRNAs to deplete 786–0 cells of either SHOC2 or PSMC1 and then assessed VSV-M51R-GFP replication relative to non-targeting (scrambled) siRNA treatments. As a positive control for enhanced VSV-M51R-GFP replication, we also included siRNA treatments targeting *relA*, which encodes a human NF-κB subunit, as NF-κB signaling has been shown to contribute to oncolytic VSV strain restriction in these cells [70]. Compared to control RNAi treatments, knockdown of RelA significantly increased VSV-M51R infection as expected. Interestingly, at least 2/3 and 3/3 siRNAs targeting SHOC2 and PSMC1, respectively, sensitized 786–0 cells to VSV-M51R-GFP infection (**Fig 7C and 7D**). Effective and specific knockdown was confirmed with immunoblotting 786–0 whole cell extracts. Notably, *SHOC2* siRNA-A was not as efficient at knocking down human SHOC2 levels and may explain why we did not detect significant differences in VSV-M51R-GFP replication in those treatments

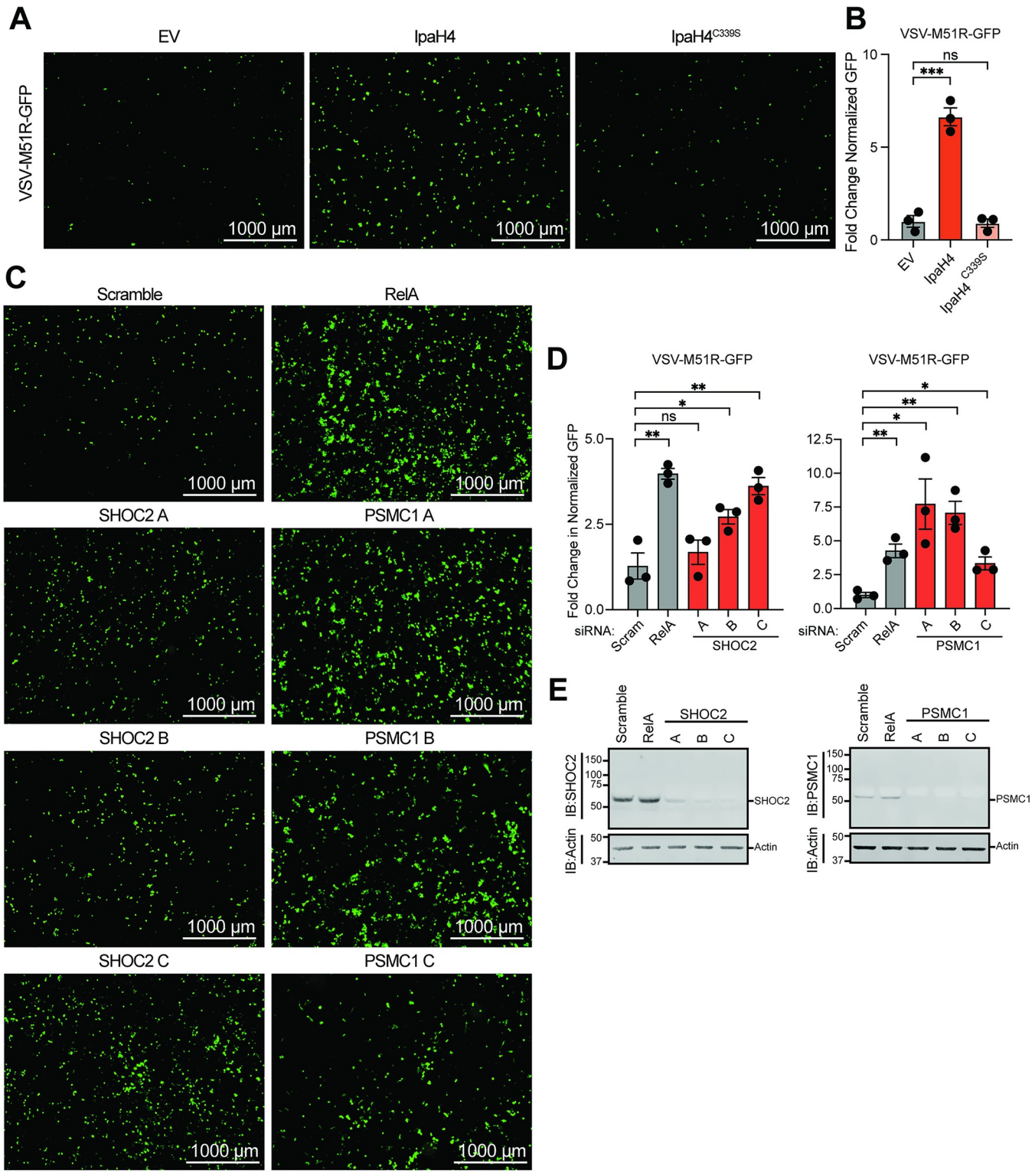

Fig 7. Bacterial effector expression or depletion of effector targets enhances oncolytic virus replication in human cancer cells. A. Representative fluorescence microscopy images (GFP channel) of human 786–0 renal adenocarcinoma cell line infected with VSV-M51R-GFP at 16 hpi. **B.** Fold-change in normalized viral GFP signal relative to empty vector (EV) control from experiments as in **A**. Cells were stained with CellTracker Orange dye 16 hpi and imaged to calculate fold-change in normalized GFP signal over EV treatments. Data are means ± SD; n = 3. Statistical significance was determined with unpaired student's t-test. **C.** Representative fluorescence microscopy images (GFP channel) of 786–0 cells infected with VSV-M51R-GFP at 16 hpi after transfection with indicated siRNAs. **D.** Fold-change in normalized viral GFP signal relative to scrambled (control) treatments as in **C**. Cells were stained with CellTracker dye 16

hpi and imaged to calculate fold-change in normalized GFP signal over control treatments. **E.** Representative immunoblot of 786–0 whole cell lysate 72 h post-transfection with indicated siRNAs. For **B** and **D**: ns = P>0.1234, * = P<0.0332, ** = P<0.0021, *** = P<0.0002, **** = P<0.0001.

https://doi.org/10.1371/journal.ppat.1012010.g007

(Fig 7E). Collectively, these data suggest that SHOC2 and PSMC1 contribute to virus restriction in human cells and suggest that they may be at least partly responsible for the refractory nature of 786–0 cells to VSV-M51R-GFP replication.

Discussion

Our study illustrates the utility of using abortive virus infections as a screening tool to identify IEPs and the host immunity factors they target. From this work, we identify a variety of bacterially-encoded proteins capable of rescuing individual arbovirus infections, as well as six that are capable of rescuing all four viruses screened. Additional analysis into the roles of these effectors showed that three of the effectors with known functions were dependent on their catalytic domains for their viral rescue phenotype. One effector of previously unknown function, Ceg10, was able to be briefly characterized through domain prediction, structure determination, and mutational analysis. Lastly, we established IpaH4 as a strong rescuer for all the arboviruses in our study, and uncovered two evolutionarily conserved targets for this E3 ubiquitin ligase: SHOC2 and PSMC1. These IpaH4 substrates were not only degraded in mammalian cell cultures, but also in invertebrate cells upon expression of wild-type, but not catalytically-inactive, IpaH4. Both SHOC2 and PSMC1 proved important for restricting arbovirus replication in LD652 insect cells and in human 786–0 cells. We envision that our screening methodology can further identify unique IEPs targeting conserved pathways for a variety of pathogen-encoded proteins.

An exciting aspect of our work is that arbovirus replication in moth LD652 cells could be rescued by 30 different bacterial effector proteins, including six (SopB, IpgD, HopAM1, HopT1-2, Ceg10 and IpaH4) that could broadly rescue all four arboviruses examined. Initial characterization of two of these effectors revealed new facets of lipid signaling involved in viral restriction. For example, our studies suggest that acute changes in the phosphorylation status of phosphatidyl inositol (PI) lipids may play a key role in viral restriction in LD652 cells. Not only do both *S. enterica*-encoded SopB and the homologous *S. flexneri*-encoded IpgD rescue arbovirus infection, but inactivation of the phosphatidylinositol phosphatase activities of these bacterial effectors abolished the viral rescue phenotype (Fig 3C-3F). There have been several reported consequences for the lipid phosphatase activity of SopB and IpgD during bacterial infection including inducing actin remodeling to promote membrane ruffling at the cell surface and bacterial entry [26,75,76] and activation of PI3K/AKT signaling to stunt programmed cell death pathways [77,78]. Interestingly, actin remodeling pathways have been shown to be critical for late stages of togavirus replication wherein these cytoskeletal arrangements are thought to mediate viral envelope protein transport to the cell surface [79]. Furthermore, many togaviruses activate PI3K/AKT signaling during infection and pharmacological inhibition of this signaling pathway has been shown to inhibit togavirus replication in vertebrate cells [80]. Although future mechanistic studies will be required to determine how exactly SopB and IpgD promote arbovirus replication in LD652 cells, it is possible that their phosphatase activity may complement a defect in the ability of these viruses to manipulate actin dynamics and/or regulate PI3K/AKT signaling pathways in these unnatural host cells.

Two unexpected hits from our screen, *P. syringae* effectors HopAM1 and HopT1-2, suggests the exciting possibility that plant pathogens can produce immune evasion factors that may disrupt host responses in both plants and invertebrate animals. *P. syringae* is a plant pathogen that has been an important model for understanding plant immunity to bacterial

infection. Recently, HopAM1 was shown to synthesize a novel cADPR variant, v2-cADPR, which has yet to be explored outside of prokaryotic and plant biology [33,34]. Our data shows that the E191 residue responsible for the ability of HopAM1 to catalyze the v2-cADPR reaction was necessary for arbovirus rescue in LD652 cells (**Fig 3C-3F**). This suggests that either the v2-ADPR molecule or NAD^+ depletion by HopAM1 may counter an innate immunity pathway important for antimicrobial responses conserved across phyla. Indeed, recent evidence suggests that some animal-encoded innate defense pathways may have originated in bacteria as antiviral defense mechanisms [81]. For example, the Thoeris system uses TIR domain-containing proteins to produce the cADPR isomer v-cADPR which triggers cell death leading to abortive phage infections in bacteria [82]. Other non-Thoeris TIR domain-containing proteins have also been implicated in a cGAS-like pathway in bacteria termed the "CBASS" pathway which also blocks phage replication [83]. Thus, our finding that HopAM1 can break virus restriction in insect cells suggests that TIR domain-containing proteins may be critical regulators of ancient antiviral defense systems used by diverse organisms. Interestingly, HopT1-2 lacks clear homology to known enzymes, but has been previously implicated in anti-bacterial immunity in plants. HopT1-2 can suppress plant nonhost resistance by inhibiting expression of nonhost 1 proteins required for activation of this immune response pathway, although how HopT1-2 achieves this function is unclear [36,37]. Nonhost resistance responses are driven by nucleotide-binding leucine-rich repeat (NLR) proteins that recognize non-adapted pathogens [36,37]. While NLR proteins are also involved in innate immune responses to pathogens in some animals, they are not conserved in insects [84]. This raises the intriguing possibility that HopT1-2 may target a conserved immune pathway shared between plant and insect hosts yet to be identified.

By far the largest proportion of effector proteins used to screen arbovirus restriction are encoded by *Legionella pneumophila*, a bacterial species that utilizes a Type IV secretion system to deliver ~350 effector proteins into the host cells. While many of these effectors exhibit unique enzymatic activities and play different roles during infection, most remain uncharacterized [85]. We found the uncharacterized *L. pneumophila*-encoded Ceg10 protein to reproducibly break viral restriction in LD652 cells. Interestingly, the conserved catalytic cysteine, Cys-159 (C159), is nitrosylated in two of our three structural data sets, indicating that this cysteine is highly reactive and particularly susceptible to oxidation by agents such as nitric oxide. Recent studies indicate that S-nitrosylation of the *Vibrio cholerae* virulence regulator AphB suppresses its enzymatic activity and alters virulence gene expression [86]. To date, of the >215,000 structures available on the Protein Data Bank, only 43 deposits display an S-nitrosothiol group, highlighting the unique nature of this modification. Furthermore, to our knowledge, Ceg10 is the first structurally characterized S-nitrosylated *Legionella* effector. We confirmed the importance of this residue by mutating C159 to serine and demonstrated that mutant Ceg10 is not capable of breaking viral restriction in LD652 cells. These data suggest that Ceg10 targets a highly conserved host restriction factor that may be important for controlling both viral and bacterial infections. Furthermore, it reveals a potential mechanism for host defense against Ceg10 via S-nitrosylation and subsequent inactivation.

While determining how SopB, IpgD, HopAM1, HopT1-2 and Ceg10 rescue virus replication in moth cells will be an exciting avenue of future research, we sought to identify novel points of viral restriction by exploring the activity of IpaH4 in greater detail given our prior interest in IpaH family members [46–48]. Through independent UBAIT- and Y2H-based screening methods, we identified host SHOC2 and PSMC1 proteins as conserved IpaH4 substrates in moth and human cells. SHOC2 is a leucine-rich repeat scaffold protein that forms a ternary complex with MRAS and PP1C that activates rapidly accelerated fibrosarcoma (RAF) kinases [87,88]. Although the specific role of SHOC2 during virus infection is unclear, it has

recently been shown to activate ERK/STAT signaling in response to bacterial flagellin in shrimp hosts [89], implying that SHOC2 may indeed have conserved roles in combating bacterial and viral pathogens. Although it is unknown if SHOC2 restricts *S. flexneri* infection, this bacterium lacks flagella. Moreover, recognition of flagella cannot explain how SHOC2 contributes to arbovirus restriction, suggesting that different pathogens can activate SHOC2-mediated immunity through distinct mechanisms. These findings highlight the strength of our system for identifying pathogen-encoded modulators of key innate immunity pathways that are likely relevant to both bacterial and viral pathogens.

PSMC1 is an essential component of the 19S cap of the proteasome functioning as one of six ATPase subunits [90]. In yeast, PSMC1 (RPT2) controls the gate of the proteasome and regulates the opening through an ATP-binding motif, allowing for substrates to enter [58]. Mutations within the ATP-binding motif in yeast PSMC1 was lethal and purified proteasomes exhibited substantially less peptidase activity [91]. Data suggests a similar role of PSMC1 in human proteasomes, although it remains unclear if other ATPase subunits are involved in gate-regulating activity [90,92]. We show that both knockdown of PSMC1 and suppression of proteasome activity alleviate the restricted arbovirus replication seen in LD652 cells. It is attractive to speculate that the proteasome degrades proteins required for the viral lifecycle in these cells, and that IpaH4 suppresses this activity resulting in viral replication. However, it is entirely possible that PSMC1-mediated virus restriction may be proteasome-dependent or -independent given the growing evidence that proteasome subunits play roles outside the proteasome complex [93–95]. Future research will be needed to address the sophisticated interaction between viral restriction and proteasome functions in the invertebrate host.

Given that the arboviruses in our study robustly replicate in human cells, we suspected that it may be more difficult to identify roles for human PSMC1 and SHOC2 in the restriction of these viruses. Thus, we sought to recapitulate a similar restricted arbovirus replication system as found in LD652 cells but in a human cell background. To do this, we took advantage of the fact that the oncolytic virotherapy strain, VSV-M51R, poorly replicates in human renal adenocarcinoma 786–0 cells due to an inability of this mutant virus to inhibit innate immune responses [62–67]. We showed that 786–0 cells became sensitive to VSV-M51R infection after either overexpression of IpaH4 or knockdown of IpaH4 substrates, PSMC1 and SHOC2 (**Fig 6**). This raises the interesting possibility that either bacterial effector function or inactivation of the host targets of effectors might enhance the replication of oncolytic viruses in cancer cell types normally refractory to these viruses. Importantly, both SHOC2 and PSMC1 are often up-regulated in human malignancies and have been linked to cellular transformation and tumor metastasis [96–98]. Indeed, gain-of-function SHOC2 mutations have been linked to RASopathies, a group of clinical pathologies associated with dysregulated RAS/MAPK signaling such as Noonan syndrome and patients with these syndromes are predisposed to certain cancers [99–101]. Moreover, elevated SHOC2 and PSMC1 expression has been associated with poorer clinical outcomes among cancer patients [98,101]. Given the common upregulation of SHOC2 and PSMC1 in transformed cells, they may be particularly relevant to the reported refractory nature of some tumors to oncolytic VSV strains replication [69,73]. Our work opens up the exciting possibility that expression of IpaH4 (or inhibition of the host factors IpaH4 targets) may provide a novel strategy for increasing oncolytic VSV strain replication in refractory tumors that, in turn, may improve virotherapy efficacy.

Limitations of the study

All high throughput screens have the potential to miss biologically relevant interactions (false-negatives) due to technical limitations. After conducting our initial effector library screens

(Fig 2) using Cellfectin II transfection reagent and pIB/V5-His-based expression vectors, we discovered that transfection with FuGENE HD and pDGOpIE2-based vectors resulted in superior transfection efficiencies in LD652 cells. Thus, it is plausible that effector proteins that require high expression levels for their function may not have been identified as hits in our initial screens. Furthermore, our study utilizes a less developed lepidopteran cell system where reagents (e.g. antibodies) that could be used to validate SHOC2 knockouts in *L. dispar* cells are not currently available. Attempts to use antibodies raised against mammalian SHOC2 failed to show cross reactivity in LD652 whole cell extract. Thus, we used multiple independent sgRNAs to confirm SHOC2-related phenotypes in insect cells. Because our focus here was on identifying host factors that contribute to virus restriction, we have not yet determined if SHOC2 or PSMC1 are targets of IpaH4 during intracellular *S. flexneri* infection. These future studies will be important for understanding the impact of IpaH4-eukaryotic host interactions to bacterial replication and pathogenesis.

Materials and methods

Cell lines and cell culture

Mammalian cell lines were maintained at 37˚C in 5% CO_2 atmosphere. HEK293T and BHK-21 cells were cultured in DMEM supplemented with 10% FBS. 786–0 cells were cultured in RPMI supplemented with 10% FBS. BSC-40 cells were cultured in MEM supplemented with 5% FBS. All media additionally contained 1% non-essential amino acids, 1% L-glutamine, and 1% antibiotic/antimycotic (Gibco). LD652 cells were cultured as described previously in a 1:1 mixture of Grace's Insect Media (Sigma) and Ex-Cell 420 (Sigma) with 10% FBS at 27˚C under normal atmospheric conditions [12].

Viruses

Stock preparation and culture of recombinant VSV and SINV was performed as previously described [12]. VSV-M51R-eGFP was obtained from Dr. Doug Lyles (Wake Forest University). RRV-GFP (strain T48), ONNV-GFP (strain SG650) constructs were obtained from Dr. John Schoggins (UTSW Medical Center). VSV, SINV, RRV, and ONNV stocks were amplified using low MOI conditions in BHK-21 cells. Viruses were collected from supernatants using ultracentrifugation (22,000 rpm, 2 h, 4˚C) and titrated on BSC-40 using fluorescent plaque/foci assays as described [12].

Viral infections were incubated for 2 h in serum free media (DMEM for mammalian cells or Sf-900 II for invertebrate cells; **S4 Table**) before the inoculum was replaced with complete media for the remainder of the infection. Where indicated, complete media containing 0.05 μg/mL ActD or 50 nM Bort was added for the remainder of the infection.

Plasmid constructs for mammalian and insect cell expression

The bacterial gene library was assembled from a previously generated pENTR library of genes [102]. Additional bacterial effector genes were added to the pENTR library by Gateway Cloning using BP Clonase II (Invitrogen; **S4 Table**), following the manufacturer's instructions. All pENTR effector genes were verified by Sanger sequencing. The entire pENTR effector library was then transferred into the pIB/V5-His vector (Invitrogen; **S4 Table**) using LR Clonase II (Invitrogen; **S4 Table**), following manufacturer's instructions.

N-terminal Flag-tagged versions of IpgD codon-optimized for expression in insect cells (NCBI accession: AAA26517.1), SopB (WFG56166.1), Ceg10 (WP_010946045.1), HopT1-2 (AA058039), and HopAM1 (Q877R9) and C-terminal Flag-tagged IpaH4 (EID62426.1) were

generated by PCR amplification using primers containing Flag sequences and flanking SacII/PacI off pIB/V5-His templates using iProof DNA polymerase (Bio-Rad; S4 Table) and cloned into the pDGOpIE2 vector. The pDGOpIE2 vector was synthesized by Gene Universal and contains an OpIE2 promoter, multiple cloning site, polyA sequence and puromycin resistance cassette. A plasmid map of the pDGOpIE2 vector can be found in S2 Fig. Catalytically-inactive mutants of IpaH4, SopB, and IpgD were constructed using site-directed mutagenesis by PCR amplification using Q5 DNA polymerase (NEB; S4 Table).

N-terminal GFP-IpaH4 was constructed through Gateway cloning into pEGFP-C2 (for mammalian expression), then PCR amplified using primers introducing SacII/PacI sites and cloned into pDGOpIE2 (for insect cell expression). C-terminal IpaH4-Flag was constructed via restriction cloning into pCDNA3. IpaH4 was PCR amplified using primers introducing SacII/PacI sites and a C-terminal Flag tag. This was then cloned into pcDNA3 (for mammalian expression).

N-terminal Flag human PSMC1 and SHOC2 were generated via Gateway cloning into pCDNA3, (for mammalian cell expression), then PCR amplified using primers introducing SacII/PacI sites and cloned into pDGOpIE2 (insect cell expression).

N-terminal Flag *L. dispar* PSMC1 and SHOC2 constructs were generated by RT-PCR amplification from total RNA isolated from LD652 cells using Superscript III reverse transcriptase (Thermo Fisher), iProof DNA polymerase, and primers containing SacII/PacI sites. SacII/PacI constructs were cloned into a modified pCDNA3 vector containing SacII/PacI sites [12] or pDGOpIE2.

General transfection and expression protocols

Unless otherwise stated, 100,000 cells were transfected with 500 ng of expression vectors and expressed for 48 h. For LD652 cell expression of the pIB/V5-His-based effector library, 500 ng of vector was mixed with 100 μL of Sf-900 media and 1.5 μL of Cellfectin II Reagent (Gibco; S4 Table). This mixture was incubated at room temperature for 20 min, and media on the cells was changed to Sf-900, then the transfection mixture was added dropwise to the well and incubated overnight. After ~16 h, media was changed to complete moth media (1:1 Grace's insect medium and EX-Cell 420 medium with 10% FBS; S4 Table) for 24 h before infection.

For later LD652 expression experiments as well as HEK293T transfection, 500 ng of vector was mixed with 50 uL of Opti-MEM and 1 μL of FuGENE HD Transfection Reagent (Promega; S4 Table). This mixture was incubated at room temperature for 20 min before adding dropwise to the well and incubated 48 h.

For 786–0 cells, vector was mixed with 50 μL of Opti-MEM and 3 μL of X-tremeGENE 9 DNA Transfection Reagent (Promega; S4 Table). This mixture was incubated at room temperature for 20 min before adding dropwise to the well and incubating 48 h.

Cell viability assay

The toxicity of the pIB/V5-His-based effector library was measured using a CyQUANT LDH Cytotoxicity assay (Invitrogen; S4 Table). Briefly, 10,000 LD652 cells per well were plated into 96-well plates and transfected the next day with the pIB/V5-His-based library (50 ng of DNA per well). Following 48 h of expression, 25 μL of supernatant media was transferred to a fresh 96-well plate and 25 μL of reaction mixtures was added to each well. The plates were mixed gently by tapping ~5 times and incubated in the dark for 30 min, then 25 μL of Stop Solution was added. The absorbance of each plate was read at both 490 nm and 680 nm within 15 min of adding Stop Solution. Data plotted indicates the 680 nm value (background signal of instrument) subtracted by the 490 nm value, per manufacturer's instructions. Controls included: an

LDH positive control provided with the kit, LD652 "media-only" negative control, and an "untransfected" cell control, and a"lysed moth cells" positive control that indicates where untransfected LD652 cells were lysed per manufacturer's instructions 1 h before collecting supernatant media.

Immunoblotting

Protein extracts were diluted in 5X SDS-PAGE loading buffer then boiled at 95˚C for 10 min. Samples were subjected to SDS-PAGE electrophoresis at 125 V for approximately 1.5 h. Separated proteins were transferred to nitrocellulose membranes in either 1X transfer buffer (BioRad; S4 Table) at 1300 mA at 25˚C, or in Towbin Buffer (BioRad; S4 Table) at 100 V at 4˚C for 100 min. Membranes were blocked in Odyssey Blocking Buffer (LI-COR; S4 Table) for 1 h at 25˚C. Membranes were blotted with primary antibody overnight at 4˚C, with actin serving as a loading control unless otherwise stated. After three, 5 min washes with PBS-T (PBS, 0.1% Tween; S4 Table), membranes were incubated in secondary antibody conjugated to an IRDye (LI-COR; S4 Table) for 1 h followed by two, 5 min washes in PBS-T and one 5 min PBS wash. Membranes were then imaged with an Odyssey Fc Imager (LI-COR; S4 Table).

Fluorescence microscopy

Cells were stained with 200 μL of serum free media containing CellTracker Orange (Invitrogen; S4 Table) dye at specified concentrations for 30 min followed by replacement with 1 mL PBS. Cells were imaged using a 2X objective on an EVOS-FL fluorescence microscope (Thermo Fisher; S4 Table) using RFP and GFP cubes. Each condition had 3 replicate wells, and two images/well were collected for analysis. Image analysis was conducted using Fiji (NIH) to quantify the percent area of each field of view containing GFP and RFP signal. Positive signal was determined by using uninfected wells lacking CellTracker stain to set a minimum threshold in both GFP and RFP channels that was applied to the remaining dataset. Only signal above the set threshold was highlighted and percent area of each field of view with fluorescent signal was measured using the Fiji analyze particles function. GFP signals were then divided by the percent area of RFP to give normalized GFP signal. Fold change in GFP signals were calculated by dividing normalized GFP values of experimental treatments with normalized GFP values in control treatments (indicated in each figure).

Structural determination of Ceg10

To determine the structured core of Ceg10 (NCBI accession: WP_010946045.1), primers were designed to clone Ceg10 into pET28b using restriction enzymes NdeI and NotI by HiFi DNA Assembly kit (NEB; S4 Table), producing the His_{6x}-TEV-Ceg10 vector. *E. coli* BL21 cells transformed with His_{6x}-TEV-Ceg10 were grown in LB medium supplemented with kanamycin (50 mg/ml). After cultures reached an OD_{600} of 0.4–0.5, protein expression was induced with 0.2 mM IPTG overnight at 18˚C. Cells were lysed using an Emulsiflex C5 (Avestin) in buffer containing 50 mM Tris-base, 500 mM sodium chloride (NaCl), 10 mM imidazole, 1 mM phenylmethylsulfonyl fluoride (PMSF), 0.5 mM tris(2-carboxyethyl)phosphine (TCEP), and SIGMAFAST Protease Inhibitor Cocktail Tablets at pH 7.0. The fusion protein was affinity purified using Ni-NTA agarose (Qiagen; S4 Table), eluted with 50 mM Tris-base, 150 mM NaCl, 250 mM imidazole, and 0.1 mM PMSF, and dialyzed overnight into 50 mM Tris-base, 150 mM NaCl, and 1 mM magnesium chloride ($MgCl_2$) at 4˚C. Limited proteolysis of Ceg10 was carried by digesting 6.4 μM His_{6x}-TEV-Ceg10 with 0.89 μM Trypsin (Sigma) in PBS. After 30 min at 25˚C, the reaction was quenched by the addition of 1 mM PMSF and the molecular

weight of the core was determined by intact mass spectroscopic analysis (UTSW Proteomic Core), revealing a highly abundant peptide (T55-R287) corresponding to residues Thr-55-Arg287 ($Ceg10^{TR}$) in Ceg10. Primers were designed to clone $Ceg10^{TR}$ pET28b as described above to produce the His_{6x}-TEV-$Ceg10^{TR}$ vector. *E. coli* BL21 cells transformed with His_{6x}-TEV-Ceg10 were grown in LB medium supplemented with kanamycin (50μg/ml). After cultures reached an OD_{600} of 0.4–0.5, protein expression was induced with 0.2 mM IPTG overnight at 18˚C. Cells were lysed using an Emulsiflex C5 (Avestin) in buffer containing 50 mM Tris-base, 500 mM NaCl, 10 mM imidazole, 1 mM PMSF, 0.5 mM TCEP, and SIGMAFAST Protease Inhibitor Cocktail Tablets at pH 7.4. The fusion protein was affinity purified using Ni-NTA agarose (Qiagen), eluted with 50 mM Tris-base, 150 mM NaCl, 250 mM imidazole, 0.5 mM TCEP and 0.1 mM PMSF, and dialyzed overnight into 50 mM Tris-base, 150 mM NaCl, and 0.5 mM TCEP at 4˚C. The 6XHis-tag was removed in the presences of 1 mM EDTA by digestion with His-tagged Tobacco Etch Virus (TEV) protease (1:50 TEV:protein ratio). After 16 h at 25˚C, $MgCl_2$ (5 mM final) was added and TEV protease was removed by passing the cleave reaction over 3 ml of Ni-NTA agarose, followed by washing with 20 ml of 10 mM Tris-base, 50 mM NaCl, and 1 mM TCEP at pH 8.0. $Ceg10^{TR}$ was concentrated to 2.5 ml using a 10,000 MWCO Amicon 50 spin concentrator, subjected to centrifugation at 40,000 rpm (TLA55 rotor), and further purified using a Superdex highload 200 16/600 gel filtration chromatography column (Cytiva Life Sciences). Fractions containing $Ceg10^{TR}$ were concentrated of 20 mg/ml and filtered with a 0.22 μm Durapore membrane filter.

Native crystals were grown by the sitting drop vapor diffusion method at 4˚C in 96-well Intelliplate trays using a 1:1 ratio of protein/reservoir solution containing 1.5 M sodium phosphate monobasic, 0.5 M potassium phosphate dibasic, 10 mM sodium phosphate dibasic/citrate buffer at pH 4.2 and were cryoprotected with 25% ethylene glycol. Native crystals diffracted to a minimum Bragg spacing (dmin) of 1.70 Å and exhibited the symmetry of space group C2221 with cell dimensions of a = 86.0 Å, b = 112.3 Å, c = 55.2 Å, and contained one $Ceg10^{55\text{-}287}$ per asymmetric unit. Crystals of S-nitrosylated $Ceg10^{55\text{-}287}$ were grown by the sitting drop vapor diffusion method at 4˚C in 96-well Intelliplate trays using a 1:1 ratio of protein/reservoir solution containing 20% PEG 1,000, 0.1 M Tris pH 7.0 and were cryoprotected with 25% ethylene glycol. S-nitrosylated $Ceg10^{55\text{-}287}$ crystals diffracted to a minimum Bragg spacing (dmin) of 1.40 Å and exhibited the symmetry of space group $P2_12_12$ with cell dimensions of a = 103.4 Å, b = 115.8 Å, c = 40.9 Å, and contained two $Ceg10^{55\text{-}287}$ per asymmetric unit. Crystals of $Ta_6Br_{12}^{2-}$ derivatized S-nitrosylated $Ceg10^{55\text{-}287}$ were grown by the sitting drop vapor diffusion method at 4˚C in 96-well Intelliplate trays using a 1:1 ratio of protein/reservoir solution containing 10% PEG 8,000, 10% PEG 1,000, 0.2 M $MgCl_2$, 0.1 M sodium acetate pH 5.0 and were cryoprotected with 25% ethylene glycol. Derivatized S-nitrosylated $Ceg10^{55\text{-}287}$ crystals diffracted to a minimum Bragg spacing (dmin) of 1.52 Å and exhibited the symmetry of space group $P2_12_12$ with cell dimensions of a = 103.6 Å, b = 116.4 Å, c = 40.8 Å, and contained two $Ceg10^{55\text{-}287}$ as well as two $Ta_6Br_{12}^{2-}$ clusters per asymmetric unit. All diffraction data were collected at beamline 19-ID (SBC-CAT) at the Advanced Photon Source (Argonne National Laboratory, Argonne, Illinois, USA) and processed in the program HKL-3000 [103] with applied corrections for effects resulting from absorption in a crystal and for radiation damage [104,105], the calculation of an optimal error model, and corrections to compensate the phasing signal for a radiation-induced increase of non-isomorphism within the crystal [106,107].

Phases were obtained from a single wavelength anomalous dispersion (SAD) experiment using the $Ta_6Br_{12}^{2-}$ derivatized S-nitrosylated $Ceg10^{55\text{-}287}$ with data to 1.52 Å collected at the LIII-edge of tantalum. Twelve tantalum sites were located by the program AutoSol, part of the Phenix package [108], and an initial model containing 78.5% of all $Ceg10^{55\text{-}287}$ residues was

automatically generated. This model was used for molecular replacement phasing of the native $Ceg10^{55-287}$ and the S-nitrosylated $Ceg10^{55-287}$. Completion of these models was performed by multiple cycles of manual rebuilding in the program Coot [109]. Positional and isotropic atomic displacement parameter (ADP) as well as TLS ADP refinement was performed using the program Phenix with a random 5.0% of all data set aside for an R_{free} calculation. Data collection and structure refinement statistics are summarized in **S2 Table**.

For determining the electrostatic potential of Ceg10 and $Ceg10^{TR}$ the APBS plugin for PyMOL (PyMOL Molecular Graphics System, Version 2.0 Schrödinger, LLC) was used.

Luciferase assay

Luciferase assays with were performed as described with minor modifications [12,22]. Briefly, at indicated times post infection/transfection, cells were washed in PBS, pelleted by brief centrifugation, and lysed in reporter lysis buffer (Promega; **S4 Table**). WCE was spotted in a 96-well dish and luciferase activity was measured in arbitrary light units (LU) using a FLUOstar Omega plate reader (BMG Labtech).

RNAi and viral infection in cell culture

Each 21-nucleotide siRNA sequence was designed based on gene prediction using LD652 genome [14] following rules established by others RNAi experiments in *Bombyx mori* [60]. siRNAs were designed against target sites that were at least 75 nts downstream of the initiation codon of each target gene, were 19 nts in length, and had a GC content of 35–55% [60]. Targets were chosen such that the sense siRNA start nucleotide was preceded by "AA" sequence and the antisense siRNA ended on an A or U [60]. Transient siRNA knockdown was achieved by forward transfection of 80,000 LD652 cells with 8 pmol siRNA and 4 μL Cellfectin II (Gibco; **S4 Table**) according to the manufacturer's protocol for 48 h prior to infection. Cells were then infected with virus for 72 h prior to imaging-based quantification of infection.

Y2H screens

Y2H screening was conducted by Hybrigenics Services (Boston, MA). The coding sequence for IpaH4 was PCR amplified from Flag-IpaH4 pCDNA3 vectors and cloned into pB66 as a C-terminal fusion to the Gal4 DNA-binding domain (but without the Flag tag) creating Gal4-IpaH4 pB66. The construct was used as a bait for two independent screens with a random-primed human lung cancer cDNA library constructed into pP6. Clones were screened at 4-fold complexity of the library using mating approach with YHGX13 (Y187 ade2-101::loxP-kanMX-loxP, mata) and CG1945 (mata) yeast strains. His+ colonies were selected on a medium lacking tryptophan, leucine and histidine. Prey fragments of the positive clones were amplified by PCR and sequenced at their 5'and 3' junctions. The resulting sequences were used to identify the corresponding interacting proteins in the GenBank database (NCBI).

UBAIT

For UBAIT assay to capture unknown substrates from cell lysates, LD652 cells were grown to confluency in three 15 cm dishes. Cells were washed with cold PBS and lysed in 300 μL 1x Ubiquitination buffer (Boston Biochem; **S4 Table**) containing 1% Triton X-100, 1x Protease inhibitor (Sigma), and 1 mM DTT. The lysate was centrifuged for 10 min at 13,000 g and 4˚C. The supernatant was transferred to a new tube before adding 25 μg of the GST-IpaH4-3xFlag-ub construct and incubating for 1 h at 4˚C with rotation. His-UbE1 (100 nM), His-UbcH5b (2000 nM), ATP (1 mM), MgCl (1 mM) and 1x Ubiquitination buffer (Boston Biochem; **S4 Table**)

were added and the reaction was incubated at 30˚C for 10 min. Following incubation, 300 μL TBS buffer (25 mM Tris-HCl pH 7.4, 150 mM NaCl, 1 mM DTT) and 30 μL of washed GST beads were added. The reaction was incubated at 4˚C for 2 h with rotation. The reaction was transferred to a column and the beads were washed four times in TBS containing 0.5% Triton-X 100 and two times in TBS before eluting in 150 μL reduced glutathione pH 8.0. Beads were centrifuged and the supernatant was transferred to a new tube followed by addition of 0.25% SDS (final concentration) and 5 mM DTT (final concentration). The solution was boiled for 5 min at 95˚C before adding 1.2 mL TBS and 20 μL M2-Flag beads (Sigma; S4 Table) and incubated at 4˚C for 2 h with rotation. Flag beads were then washed four times in TBS containing 0.5% Triton X-100 and twice with TBS. Finally, 35 μL of 95˚C SDS-PAGE loading buffer was added, and the beads were boiled an additional 5 min at 95˚C. Samples were subjected to SDS-PAGE and Coomassie stained. To identify captured proteins, a lane of the gel above the unmodified IpaH4-UBAIT band was excised and proteins were digested in-gel with trypsin and run on a Q Exactive MS platform at the University of Texas Southwestern Medical Center Proteomics Core.

Degradation assay

100,000 HEK-293T cells were co-transfected with 150 ng GFP/GFP-IpaH4/GFP-IpaH4^{C339S} and 350 ng target vectors for 48 h using FuGENE (Promega; S4 Table). Cells were harvested in RIPA buffer containing 100 μM PMSF and protease inhibitor cocktail (Abcam; S4 Table). Protein extracts were then subjected to SDS-PAGE and subsequent immunoblotting as indicated in each figure.

Protein purification

To obtain C-terminal 5XHis-tagged PSMC1, human *PSMC1* was cloned into pET21a by restriction cloning with NdeI/XhoI and expressed in *E. coli* BL21in the presence of ampicillin. After the cultures reached OD_{600} 0.7, protein expression was induced with 0.5 mM IPTG at 18˚C overnight. Cells were lysed using an Emulsiflex C5 (Avestin) in buffer containing 25 mM HEPES, 100 mM NaCl, 100 mM KCl, 10% glycerol, 10 mM $MgCl_2$, 0.5 mM EDTA, 1 mM DTT, and 10 mM Imidazole (HBSi; S4 Table) with the final pH at 7.5. The fusion protein was affinity-purified using TALON Metal Affinity Resin (Takara Biosciences; S4 Table) and eluted in buffer containing 25 mM HEPES, 100 mM NaCl, 100 mM KCl, 10% glycerol, 10 mM $MgCl_2$, 0.5 mM EDTA, 1 mM DTT, and 500 mM Imidazole. The protein was dialyzed using a 10,000 MWCO Slide-A-Lyzer G3 dialysis cassette (Thermo S4 Table) in 1 L of buffer containing 25 mM HEPES, 100 mM NaCl, 100 mM KCl, 10% glycerol, 10 mM $MgCl_2$, 0.5 mM EDTA, 1 mM DTT.

To obtain N-terminal 6XHis-MBP-TEV-Flag-tagged SHOC2, *E. coli* carrying pET28a-SHOC2 were grown in LB media supplemented with ampicillin. After the cultures reached OD_{600} 0.7, protein expression was induced with 0.5 mM IPTG at 17˚C overnight. Cells were lysed by sonication with 5 second pulses and 20 second intervals for 50 min at 4˚C in buffer containing 50 mM Tris-HCl, 150 mM NaCl, 1 mM TCEP, 1 mM PMSF, and 20 mM Imidazole (HBSi) with the final pH at 8. The lysate was then subjected to centrifugation at 10,000 x g for 30 min at 4˚C. The fusion protein was affinity-purified using TALON metal affinity resin (Takara Biosciences) and eluted in buffer containing 50 mM Tris-HCl, 150 mM NaCl, 1 mM TCEP, 0.1 mM PMSF, and 250 mM Imidazole. The protein was concentrated using a 30,000 MWCO Amicon 50 spin concentrator then dialyzed using a 10,000 MWCO Slide-A-Lyzer G3 dialysis cassette (Thermo) in buffer containing 25 mM Tris-HCl and 75 mM NaCl. Flag-SHOC2 was cleaved from 6X-His-MBP by incubating 37 mg purified protein with 0.65 mg

TEV protease at 4˚C overnight followed by affinity purification using Nickel affinity resin (Qiagen) where cleaved Flag-SHOC2 was collected in the flow-through.

Recombinant GST-IpaH4-3XFlag for UBAIT experiments was obtained as previously described for other IpaH proteins [46,110]. Briefly, GST-IpaH4-3XFlag was cloned into pGEX6P-1 with a 3XFlag peptide followed by the coding sequence for ubiquitin using Gibson Cloning (NEB; **S4 Table**). Sequence-verified constructs were transformed into *E. coli* BL21 cells, induced, and recombinant protein was purified using glutathione sepharose beads (GE Healthcare Life Sciences).

Recombinant GST-IpaH4 for *in vitro* experiments was expressed and purified as previously described for other IpaH proteins [46,110]. Briefly, GST-IpaH4 was cloned into pGEX6P-1, transformed into *E. coli* BL21 cells, induced, and recombinant protein was purified using glutathione sepharose beads (GE Healthcare Life Sciences; **S4 Table**).

In-vitro ubiquitination assay

In vitro ubiquitination reactions were performed in 50 mM HEPES pH 7.5, 150 mM NaCl, 20 mM $MgCl_2$, and 10 mM ATP (47). Components were mixed as indicated at the following concentrations 1 μM UbE1 (E1), 5 μM UbcH5b (E2), 500 nM-10 μM GST-IpaH or GST-IpaH4^{C339S}, 50 μM ubiquitin, and 5 μM His-tagged PSMC1, or 5 μM Flag-tagged SHOC2. Reactions were incubated for 18 h at 30˚C before the addition of 2X loading buffer containing β-mercaptoethanol (BME). Samples were then boiled for 10 min at 95˚C, subjected to SDS-PAGE, and immunoblotted with anti-GST, anti-Ubiquitin, anti-His or anti-Flag antibodies.

Statistical analysis

Graphs and charts were presented as mean values ± standard error of mean (SEM) with individual data points for each independent experiment shown. At least three independent experiments were conducted for all quantitative experiments shown. All statistical analyses were performed with Prism software v10.0.2 (GraphPad) and statistical tests used are indicated in respective figure legends. Statistical significance ($P<0.05$) between compared groups is indicated in figures as either: ns (not significant), * = $P<0.05$, ** = $P<0.01$, *** = $P<0.001$, **** = $P<0.0001$.

Supporting information

S1 Table. Bacterial effector library screening results and cell viability data.
(XLSX)

S2 Table. Data collection and refinement statistics, Ceg10 structures.
(XLSX)

S3 Table. Identification of IpaH4 substrates.
(XLSX)

S4 Table. Key resources and reagents.
(XLSX)

S5 Table. Raw data.
(XLSX)

S1 Fig. LD652 cell viability upon expression of pIB/V5-His-based effector library. A-C. Absorbance at 490 nm for supernatant collected from LD652 cells expressing the pIB/V5-His-

based effector library for 48 h. Source data for cell viability assays are available in S1 Table.
(TIF)

S2 Fig. Generation of insect expression vector pDGOpIE2. A. Snapgene vector map of pDGOpIE2 vector and features of interest. **B.** Complete sequence of pDGOpIE2 vector.
(TIF)

S3 Fig. LD652 cell viability upon expression of pDGOpIE2 effectors. Absorbance at 490 nm for supernatants collected from LD652 cells transfected with the indicated pDGOpIE2 effector expression vectors for 48 h.
(TIF)

S4 Fig. Identification of putative targets of bacterial E3 ubiquitin ligase IpaH4. A. Table summarizing results of two independent Y2H screens using a human prey library and three independent ubiquitin-activated interaction trap (UBAIT) assays using LD652 cell lysate. Hits were then analyzed via Blastp to determine percent identity to their *Homo sapiens* ortholog. N.D. = Not determined; either no ortholog found or no significant homology (as determined by BLAST). (B) Representative immunoblot of degradation assays for Flag-tagged human proteins following 48 h co-expression in HEK293T cells with GFP, IpaH4 (WT) or catalytic mutant GST-IpaH4C339S (C339S).
(TIF)

S5 Fig. Establishing siRNA knockdown conditions in LD652 cells. A. Schematic detailing siRNA knockdown protocol in LD652 cells. Image was created with BioRender.com. **B.** Relative Light Units (RLU) of LD652 lysates from cells transfected with empty vector (EV) or luciferase (Luc)-expressing vectors for 48 h and then transfected with siRNA targeting LacZ (negative control) or Luc sequences for 48 h. **C.** Representative immunoblot of PSMC1 knockdown following 48 h for siRNA treatment with duplexes targeting LacZ, AGO-2, or PSMC1.
(TIF)

S6 Fig. Proteasomal activity plays a role in restricting arbovirus replication in LD652 cells. A. Representative fluorescence microscopy images (GFP channel) of LD652 cells 72 hpi with the indicated GFP reporter strains that were treated with DMSO (vehicle) or 50 nM Bortezomib (Bort). DMSO or Bort was added 2 hpi. **B.** Fold-change in normalized GFP signals in Bort-treated cultures relative to DMSO treatments. Cells were stained 72 hpi with CellTracker Orange dye (not shown) and imaged in GFP and RFP channels to calculate fold-change in GFP signal after normalization of cell number using CellTracker (RFP) channel signals. Data are means ± SD; n = 3. Statistical significance was determined with unpaired student's t-test; ns = $P>0.1234$, * = $P<0.0332$, ** = $P<0.0021$, *** = $P<0.0002$, **** = $P<0.0001$.
(TIF)

Acknowledgments

We would like to thank Drs. John Schoggins and Andrew Sandstrom (UT Southwestern Medical Center) and members of the Gammon and Alto laboratories for helpful discussions. We also thank Dr. Don Jarvis (University of Wyoming) for providing the pIE1-Cas9-SfU6-sgRNA-Puro vector. We thank the UT Southwestern Medical Center Proteomics Core for assistance with aspects of experimental execution. Results shown in this report are derived from work performed at Argonne National Laboratory (ANL), Structural Biology Center (SBC) at the Advanced Photon Source (APS), under U.S. Department of Energy, Office of Biological and Environmental Research contract DE-AC02-06CH11357. We thank the Structural

Biology Laboratory at UT Southwestern Medical Center for support with X-ray crystallographic studies.

Author Contributions

Conceptualization: Aaron Embry, Nina S. Baggett, David B. Heisler, Neal M. Alto, Don B. Gammon.

Data curation: Aaron Embry, Nina S. Baggett, David B. Heisler, Addison White, Maarten F. de Jong, Diana R. Tomchick, Don B. Gammon.

Formal analysis: Aaron Embry, Diana R. Tomchick, Neal M. Alto, Don B. Gammon.

Funding acquisition: Aaron Embry, Nina S. Baggett, Neal M. Alto, Don B. Gammon.

Investigation: Aaron Embry, Nina S. Baggett, David B. Heisler, Addison White, Maarten F. de Jong, Benjamin L. Kocsis, Diana R. Tomchick, Don B. Gammon.

Methodology: Aaron Embry, Nina S. Baggett, David B. Heisler, Diana R. Tomchick, Neal M. Alto, Don B. Gammon.

Project administration: Neal M. Alto, Don B. Gammon.

Resources: David B. Heisler, Maarten F. de Jong, Benjamin L. Kocsis.

Supervision: Neal M. Alto, Don B. Gammon.

Validation: Nina S. Baggett, Don B. Gammon.

Visualization: Aaron Embry, Nina S. Baggett, Diana R. Tomchick, Neal M. Alto, Don B. Gammon.

Writing – original draft: Aaron Embry, Nina S. Baggett, David B. Heisler, Diana R. Tomchick, Don B. Gammon.

Writing – review & editing: Aaron Embry, Nina S. Baggett, David B. Heisler, Addison White, Neal M. Alto, Don B. Gammon.

References

1. Velazquez-Salinas L, Pauszek SJ, Stenfeldt C, O'Hearn ES, Pacheco JM, Borca MV, et al. Increased Virulence of an Epidemic Strain of Vesicular Stomatitis Virus Is Associated With Interference of the Innate Response in Pigs. Front Microbiol. 2018; 9:1891. Epub 2018/08/31. https://doi.org/10.3389/fmicb.2018.01891 PMID: 30158915; PubMed Central PMCID: PMC6104175.
2. Madewell ZJ. Arboviruses and Their Vectors. South Med J. 2020; 113(10):520–3. Epub 2020/10/03. https://doi.org/10.14423/SMJ.0000000000001152 PMID: 33005970; PubMed Central PMCID: PMC8055094.
3. Balakrishnan VS. WHO launches global initiative for arboviral diseases. Lancet Microbe. 2022; 3(6): e407. Epub 2022/06/07. https://doi.org/10.1016/S2666-5247(22)00130-6 PMID: 35659901; PubMed Central PMCID: PMC9159734.
4. Guerrero-Arguero I, Tellez-Freitas CM, Weber KS, Berges BK, Robison RA, Pickett BE. Alphaviruses: Host pathogenesis, immune response, and vaccine & treatment updates. J Gen Virol. 2021; 102(8). Epub 2021/08/27. https://doi.org/10.1099/jgv.0.001644 PMID: 34435944.
5. Abdelnabi R, Delang L. Antiviral Strategies against Arthritogenic Alphaviruses. Microorganisms. 2020; 8(9). Epub 2020/09/11. https://doi.org/10.3390/microorganisms8091365 PMID: 32906603; PubMed Central PMCID: PMC7563460.
6. Kirby EN, Shue B, Thomas PQ, Beard MR. CRISPR Tackles Emerging Viral Pathogens. Viruses. 2021; 13(11). Epub 2021/11/28. https://doi.org/10.3390/v13112157 PMID: 34834963; PubMed Central PMCID: PMC8624524.

7. Kanojia A, Sharma M, Shiraz R, Tripathi S. Flavivirus-Host Interaction Landscape Visualized through Genome-Wide CRISPR Screens. Viruses. 2022; 14(10). Epub 2022/10/28. https://doi.org/10.3390/v14102164 PMID: 36298718; PubMed Central PMCID: PMC9609550.

8. Yasunaga A, Hanna SL, Li J, Cho H, Rose PP, Spiridigliozzi A, et al. Genome-wide RNAi screen identifies broadly-acting host factors that inhibit arbovirus infection. PLoS Pathog. 2014; 10(2):e1003914. Epub 2014/02/20. https://doi.org/10.1371/journal.ppat.1003914 PMID: 24550726; PubMed Central PMCID: PMC3923753.

9. Salomon D, Orth K. What pathogens have taught us about posttranslational modifications. Cell Host Microbe. 2013; 14(3):269–79. Epub 2013/09/17. https://doi.org/10.1016/j.chom.2013.07.008 PMID: 24034613; PubMed Central PMCID: PMC5785091.

10. Mak H, Thurston TLM. Interesting Biochemistries in the Structure and Function of Bacterial Effectors. Front Cell Infect Microbiol. 2021; 11:608860. Epub 2021/03/16. https://doi.org/10.3389/fcimb.2021.608860 PMID: 33718265; PubMed Central PMCID: PMC7943720.

11. Zhu J, Chiang C, Gack MU. Viral evasion of the interferon response at a glance. J Cell Sci. 2023; 136 (12). Epub 2023/06/21. https://doi.org/10.1242/jcs.260682 PMID: 37341132; PubMed Central PMCID: PMC10411950.

12. Gammon DB, Duraffour S, Rozelle DK, Hehnly H, Sharma R, Sparks ME, et al. A single vertebrate DNA virus protein disarms invertebrate immunity to RNA virus infection. Elife. 2014;3. Epub 2014/06/27. https://doi.org/10.7554/eLife.02910 PMID: 24966209; PubMed Central PMCID: PMC4112549.

13. Embry A, Gammon D.B.Abortive Infection of Animal Cells: What Goes Wrong. Annual Review of Virology. 2024; 11. Epub In Press. In Press. https://doi.org/10.1146/annurev-virology-100422-023037 PMID: 38631917

14. Zhang J, Cong Q, Rex EA, Hallwachs W, Janzen DH, Grishin NV, et al. Gypsy moth genome provides insights into flight capability and virus-host interactions. Proc Natl Acad Sci U S A. 2019; 116(5):1669–78. Epub 2019/01/16. https://doi.org/10.1073/pnas.1818283116 PMID: 30642971; PubMed Central PMCID: PMC6358702.

15. de Jong MF, Alto NM. Cooperative Immune Suppression by Escherichia coli and Shigella Effector Proteins. Infect Immun. 2018; 86(4). Epub 2018/01/18. https://doi.org/10.1128/IAI.00560-17 PMID: 29339461; PubMed Central PMCID: PMC5865018.

16. Alphonse N, Dickenson RE, Odendall C. Interferons: Tug of War Between Bacteria and Their Host. Front Cell Infect Microbiol. 2021; 11:624094. Epub 2021/03/30. https://doi.org/10.3389/fcimb.2021.624094 PMID: 33777837; PubMed Central PMCID: PMC7988231.

17. Chen D, Burford WB, Pham G, Zhang L, Alto LT, Ertelt JM, et al. Systematic reconstruction of an effector-gene network reveals determinants of Salmonella cellular and tissue tropism. Cell Host Microbe. 2021; 29(10):1531–44 e9. Epub 2021/09/19. https://doi.org/10.1016/j.chom.2021.08.012 PMID: 34536347; PubMed Central PMCID: PMC8516738.

18. Sobell HM. Actinomycin and DNA transcription. Proc Natl Acad Sci U S A. 1985; 82(16):5328–31. Epub 1985/08/01. https://doi.org/10.1073/pnas.82.16.5328 PMID: 2410919; PubMed Central PMCID: PMC390561.

19. Kang HJ, Park HJ. Novel molecular mechanism for actinomycin D activity as an oncogenic promoter G-quadruplex binder. Biochemistry. 2009; 48(31):7392–8. Epub 2009/06/06. https://doi.org/10.1021/bi9006836 PMID: 19496619.

20. Morrison TE, Whitmore AC, Shabman RS, Lidbury BA, Mahalingam S, Heise MT. Characterization of Ross River virus tropism and virus-induced inflammation in a mouse model of viral arthritis and myositis. J Virol. 2006; 80(2):737–49. Epub 2005/12/28. https://doi.org/10.1128/JVI.80.2.737-749.2006 PMID: 16378976; PubMed Central PMCID: PMC1346871.

21. Brault AC, Foy BD, Myles KM, Kelly CL, Higgs S, Weaver SC, et al. Infection patterns of o'nyong nyong virus in the malaria-transmitting mosquito, Anopheles gambiae. Insect Mol Biol. 2004; 13 (6):625–35. Epub 2004/12/21. https://doi.org/10.1111/j.0962-1075.2004.00521.x PMID: 15606811.

22. Rex EA, Seo D, Gammon DB. Arbovirus Infections As Screening Tools for the Identification of Viral Immunomodulators and Host Antiviral Factors. J Vis Exp. 2018;(139). Epub 20180913. https://doi.org/10.3791/58244 PMID: 30272671; PubMed Central PMCID: PMC6235183.

23. Weigele BA, Orchard RC, Jimenez A, Cox GW, Alto NM. A systematic exploration of the interactions between bacterial effector proteins and host cell membranes. Nature Communications. 2017; 8 (1):532. https://doi.org/10.1038/s41467-017-00700-7 PMID: 28912547

24. Theilmann DA, Stewart S. Molecular analysis of the trans-activating IE-2 gene of Orgyia pseudotsugata multicapsid nuclear polyhedrosis virus. Virology. 1992; 187(1):84–96. Epub 1992/03/01. https://doi.org/10.1016/0042-6822(92)90297-3 PMID: 1736546.

25. Norris FA, Wilson MP, Wallis TS, Galyov EE, Majerus PW. SopB, a protein required for virulence of Salmonella dublin, is an inositol phosphate phosphatase. Proceedings of the National Academy of Sciences. 1998; 95(24):14057–9. https://doi.org/10.1073/pnas.95.24.14057 PMID: 9826652

26. Piscatelli HL, Li M, Zhou D. Dual 4- and 5-phosphatase activities regulate SopB-dependent phosphoinositide dynamics to promote bacterial entry. Cellular Microbiology. 2016; 18(5):705–19. https://doi.org/10.1111/cmi.12542 PMID: 26537021

27. Dukes JD, Lee H, Hagen R, Reaves BJ, Layton AN, Galyov EE, et al. The secreted Salmonella dublin phosphoinositide phosphatase, SopB, localizes to PtdIns(3)P-containing endosomes and perturbs normal endosome to lysosome trafficking. Biochem J. 2006; 395(2):239–47. https://doi.org/10.1042/BJ20051451 PMID: 16396630; PubMed Central PMCID: PMC1422764.

28. Norris FA, Wilson MP, Wallis TS, Galyov EE, Majerus PW. SopB, a protein required for virulence of Salmonella dublin, is an inositol phosphate phosphatase. Proc Natl Acad Sci U S A. 1998; 95 (24):14057–9. Epub 1998/11/25. https://doi.org/10.1073/pnas.95.24.14057 PMID: 9826652; PubMed Central PMCID: PMC24325.

29. Zhou D, Chen LM, Hernandez L, Shears SB, Galan JE. A Salmonella inositol polyphosphatase acts in conjunction with other bacterial effectors to promote host cell actin cytoskeleton rearrangements and bacterial internalization. Mol Microbiol. 2001; 39(2):248–59. Epub 2001/01/03. https://doi.org/10.1046/j.1365-2958.2001.02230.x PMID: 11136447.

30. Niebuhr K, Giuriato S, Pedron T, Philpott DJ, Gaits F, Sable J, et al. Conversion of PtdIns(4,5)P(2) into PtdIns(5)P by the S.flexneri effector IpgD reorganizes host cell morphology. Embo j. 2002; 21 (19):5069–78. https://doi.org/10.1093/emboj/cdf522 PMID: 12356723; PubMed Central PMCID: PMC129044.

31. Garza-Mayers AC, Miller KA, Russo BC, Nagda DV, Goldberg MB. Shigella flexneri Regulation of ARF6 Activation during Bacterial Entry via an IpgD-Mediated Positive Feedback Loop. mBio. 2015; 6 (2):10.1128/mbio.02584-14. https://doi.org/10.1128/mBio.02584-14 PMID: 25736891

32. Bakowski MA, Braun V, Lam GY, Yeung T, Heo WD, Meyer T, et al. The phosphoinositide phosphatase SopB manipulates membrane surface charge and trafficking of the Salmonella-containing vacuole. Cell Host Microbe. 2010; 7(6):453–62. Epub 2010/06/15. https://doi.org/10.1016/j.chom.2010.05.011 PMID: 20542249.

33. Eastman S, Smith T, Zaydman MA, Kim P, Martinez S, Damaraju N, et al. A phytobacterial TIR domain effector manipulates NAD+ to promote virulence. New Phytologist. 2022; 233(2):890–904. https://doi.org/10.1111/nph.17805 PMID: 34657283

34. Manik MK, Shi Y, Li S, Zaydman MA, Damaraju N, Eastman S, et al. Cyclic ADP ribose isomers: Production, chemical structures, and immune signaling. Science. 2022; 377(6614):eadc8969. https://doi.org/10.1126/science.adc8969 PMID: 36048923

35. Eastman S, Smith T, Zaydman MA, Kim P, Martinez S, Damaraju N, et al. A phytobacterial TIR domain effector manipulates NAD(+) to promote virulence. New Phytol. 2022; 233(2):890–904. Epub 2021/10/18. https://doi.org/10.1111/nph.17805 PMID: 34657283; PubMed Central PMCID: PMC9298051.

36. Oh S, Choi D. Receptor-mediated nonhost resistance in plants. Essays Biochem. 2022; 66(5):435–45. Epub 2022/04/08. https://doi.org/10.1042/EBC20210080 PMID: 35388900; PubMed Central PMCID: PMC9528085.

37. Li X, Lin H, Zhang W, Zou Y, Zhang J, Tang X, et al. Flagellin induces innate immunity in nonhost interactions that is suppressed by Pseudomonas syringae effectors. Proc Natl Acad Sci U S A. 2005; 102 (36):12990–5. Epub 20050825. https://doi.org/10.1073/pnas.0502425102 PMID: 16123135; PubMed Central PMCID: PMC1200263.

38. Soding J, Biegert A, Lupas AN. The HHpred interactive server for protein homology detection and structure prediction. Nucleic Acids Res. 2005; 33(Web Server issue):W244-8. Epub 2005/06/28. https://doi.org/10.1093/nar/gki408 PMID: 15980461; PubMed Central PMCID: PMC1160169.

39. Leseigneur C, Buchrieser C. Modelling Legionnaires' disease: Lessons learned from invertebrate and vertebrate animal models. Eur J Cell Biol. 2023; 102(4):151369. Epub 2023/11/06. https://doi.org/10.1016/j.ejcb.2023.151369 PMID: 37926040.

40. Krissinel E, Henrick K. Secondary-structure matching (SSM), a new tool for fast protein structure alignment in three dimensions. Acta Crystallogr D Biol Crystallogr. 2004; 60(Pt 12 Pt 1):2256–68. Epub 20041126. https://doi.org/10.1107/S0907444904026460 PMID: 15572779.

41. Fernando V, Zheng X, Walia Y, Sharma V, Letson J, Furuta S. S-Nitrosylation: An Emerging Paradigm of Redox Signaling. Antioxidants (Basel). 2019; 8(9). Epub 20190917. https://doi.org/10.3390/antiox8090404 PMID: 31533268; PubMed Central PMCID: PMC6769533.

42. Helen R. Swift DLHW. Decomposition of S-nitrosothiols by mercury(II) and silver salts. J Chem Soc, Perkin Trans 2. 1997:1933–5. https://doi.org/10.1039/A702937C

43. Alphonse N, Odendall C. Animal models of shigellosis: a historical overview. Curr Opin Immunol. 2023; 85:102399. Epub 2023/11/13. https://doi.org/10.1016/j.coi.2023.102399 PMID: 37952487.

44. Zhu Y, Li H, Hu L, Wang J, Zhou Y, Pang Z, et al. Structure of a Shigella effector reveals a new class of ubiquitin ligases. Nat Struct Mol Biol. 2008; 15(12):1302–8. Epub 2008/11/11. https://doi.org/10.1038/nsmb.1517 PMID: 18997779.

45. Singer AU, Rohde JR, Lam R, Skarina T, Kagan O, Dileo R, et al. Structure of the Shigella T3SS effector IpaH defines a new class of E3 ubiquitin ligases. Nat Struct Mol Biol. 2008; 15(12):1293–301. Epub 2008/11/11. https://doi.org/10.1038/nsmb.1511 PMID: 18997778; PubMed Central PMCID: PMC2764551.

46. de Jong MF, Liu Z, Chen D, Alto NM. Shigella flexneri suppresses NF-kappaB activation by inhibiting linear ubiquitin chain ligation. Nat Microbiol. 2016; 1(7):16084. Epub 2016/08/31. https://doi.org/10.1038/nmicrobiol.2016.84 PMID: 27572974; PubMed Central PMCID: PMC5010086.

47. Hansen JM, de Jong MF, Wu Q, Zhang LS, Heisler DB, Alto LT, et al. Pathogenic ubiquitination of GSDMB inhibits NK cell bactericidal functions. Cell. 2021; 184(12):3178–91 e18. Epub 2021/05/23. https://doi.org/10.1016/j.cell.2021.04.036 PMID: 34022140; PubMed Central PMCID: PMC8221529.

48. Yin H, Zheng J, He Q, Zhang X, Li X, Ma Y, et al. Insights into the GSDMB-mediated cellular lysis and its targeting by IpaH7.8. Nat Commun. 2023; 14(1):61. Epub 2023/01/05. https://doi.org/10.1038/s41467-022-35725-0 PMID: 36599845; PubMed Central PMCID: PMC9813358.

49. Rohde JR, Breitkreutz A, Chenal A, Sansonetti PJ, Parsot C. Type III secretion effectors of the IpaH family are E3 ubiquitin ligases. Cell Host Microbe. 2007; 1(1):77–83. Epub 2007/11/17. https://doi.org/10.1016/j.chom.2007.02.002 PMID: 18005683.

50. Ashida H, Nakano H, Sasakawa C. Shigella IpaH0722 E3 ubiquitin ligase effector targets TRAF2 to inhibit PKC-NF-kappaB activity in invaded epithelial cells. PLoS Pathog. 2013; 9(6):e1003409. Epub 2013/06/12. https://doi.org/10.1371/journal.ppat.1003409 PMID: 23754945; PubMed Central PMCID: PMC3675035.

51. Fang S, Weissman AM. A field guide to ubiquitylation. Cell Mol Life Sci. 2004; 61(13):1546–61. Epub 2004/06/30. https://doi.org/10.1007/s00018-004-4129-5 PMID: 15224180.

52. Blount JR, Johnson SL, Todi SV. Unanchored Ubiquitin Chains, Revisited. Front Cell Dev Biol. 2020; 8:582361. Epub 2020/11/17. https://doi.org/10.3389/fcell.2020.582361 PMID: 33195227; PubMed Central PMCID: PMC7659471.

53. O'Connor HF, Lyon N, Leung JW, Agarwal P, Swaim CD, Miller KM, et al. Ubiquitin-Activated Interaction Traps (UBAITs) identify E3 ligase binding partners. EMBO Rep. 2015; 16(12):1699–712. Epub 2015/10/29. https://doi.org/10.15252/embr.201540620 PMID: 26508657; PubMed Central PMCID: PMC4693525.

54. Keszei AF, Sicheri F. Mechanism of catalysis, E2 recognition, and autoinhibition for the IpaH family of bacterial E3 ubiquitin ligases. Proc Natl Acad Sci U S A. 2017; 114(6):1311–6. Epub 2017/01/25. https://doi.org/10.1073/pnas.1611595114 PMID: 28115697; PubMed Central PMCID: PMC5307447.

55. Chou YC, Keszei AFA, Rohde JR, Tyers M, Sicheri F. Conserved structural mechanisms for autoinhibition in IpaH ubiquitin ligases. J Biol Chem. 2012; 287(1):268–75. Epub 2011/11/09. https://doi.org/10.1074/jbc.M111.316265 PMID: 22065585; PubMed Central PMCID: PMC3249077.

56. O'Connor HF, Swaim CD, Canadeo LA, Huibregtse JM. Ubiquitin-Activated Interaction Traps (UBAITs): Tools for Capturing Protein-Protein Interactions. Methods Mol Biol. 2018; 1844:85–100. Epub 2018/09/23. https://doi.org/10.1007/978-1-4939-8706-1_7 PMID: 30242705.

57. Mabashi-Asazuma H, Jarvis DL. CRISPR-Cas9 vectors for genome editing and host engineering in the baculovirus–insect cell system. Proceedings of the National Academy of Sciences. 2017; 114(34):9068–73. https://doi.org/10.1073/pnas.1705836114 PMID: 28784806

58. Rubin DM, Glickman MH, Larsen CN, Dhruvakumar S, Finley D. Active site mutants in the six regulatory particle ATPases reveal multiple roles for ATP in the proteasome. Embo j. 1998; 17(17):4909–19. https://doi.org/10.1093/emboj/17.17.4909 PMID: 9724628; PubMed Central PMCID: PMC1170820.

59. Kaneko T, Hamazaki J, Iemura S-i, Sasaki K, Furuyama K, Natsume T, et al. Assembly Pathway of the Mammalian Proteasome Base Subcomplex Is Mediated by Multiple Specific Chaperones. Cell. 2009; 137(5):914–25. https://doi.org/10.1016/j.cell.2009.05.008 PMID: 19490896

60. Yamaguchi J, Mizoguchi T, Fujiwara H. siRNAs Induce Efficient RNAi Response in Bombyx mori Embryos. PLOS ONE. 2011; 6(9):e25469. https://doi.org/10.1371/journal.pone.0025469 PMID: 21980469

61. Kingsolver MB, Huang Z, Hardy RW. Insect antiviral innate immunity: pathways, effectors, and connections. J Mol Biol. 2013; 425(24):4921–36. Epub 20131009. https://doi.org/10.1016/j.jmb.2013.10.006 PMID: 24120681; PubMed Central PMCID: PMC4007215.

62. Yuan H, Yoza BK, Lyles DS. Inhibition of Host RNA Polymerase II-Dependent Transcription by Vesicular Stomatitis Virus Results from Inactivation of TFIID. Virology. 1998; 251(2):383–92. https://doi.org/10.1006/viro.1998.9413 PMID: 9837802

63. von Kobbe C, van Deursen JMA, Rodrigues JP, Sitterlin D, Bachi A, Wu X, et al. Vesicular Stomatitis Virus Matrix Protein Inhibits Host Cell Gene Expression by Targeting the Nucleoporin Nup98. Molecular Cell. 2000; 6(5):1243–52. https://doi.org/10.1016/s1097-2765(00)00120-9 PMID: 11106761

64. Faria PA, Chakraborty P, Levay A, Barber GN, Ezelle HJ, Enninga J, et al. VSV Disrupts the Rae1/mrnp41 mRNA Nuclear Export Pathway. Molecular Cell. 2005; 17(1):93–102. https://doi.org/10.1016/j.molcel.2004.11.023 PMID: 15629720

65. Black BL, Lyles DS. Vesicular stomatitis virus matrix protein inhibits host cell-directed transcription of target genes in vivo. Journal of Virology. 1992; 66(7):4058–64. https://doi.org/10.1128/JVI.66.7.4058-4064.1992 PMID: 1318397

66. Ahmed M, McKenzie MO, Puckett S, Hojnacki M, Poliquin L, Lyles DS. Ability of the Matrix Protein of Vesicular Stomatitis Virus To Suppress Beta Interferon Gene Expression Is Genetically Correlated with the Inhibition of Host RNA and Protein Synthesis. Journal of Virology. 2003; 77(8):4646–57. https://doi.org/10.1128/jvi.77.8.4646-4657.2003 PMID: 12663771

67. Marquis KA, Becker RL, Weiss AN, Morris MC, Ferran MC. The VSV matrix protein inhibits NF-κB and the interferon response independently in mouse L929 cells. Virology. 2020; 548:117–23. https://doi.org/10.1016/j.virol.2020.06.013.

68. Blackham AU, Northrup SA, Willingham M, D'Agostino RB Jr., Lyles DS, Stewart JHt. Variation in susceptibility of human malignant melanomas to oncolytic vesicular stomatitis virus. Surgery. 2013; 153(3):333–43. Epub 20121025. https://doi.org/10.1016/j.surg.2012.09.003 PMID: 23102637; PubMed Central PMCID: PMC3561511.

69. Holbrook MC, Goad DW, Grdzelishvili VZ. Expanding the Spectrum of Pancreatic Cancers Responsive to Vesicular Stomatitis Virus-Based Oncolytic Virotherapy: Challenges and Solutions. Cancers (Basel). 2021; 13(5). Epub 2021/04/04. https://doi.org/10.3390/cancers13051171 PMID: 33803211; PubMed Central PMCID: PMC7963195.

70. Selman M, Ou P, Rousso C, Bergeron A, Krishnan R, Pikor L, et al. Dimethyl fumarate potentiates oncolytic virotherapy through NF-kappaB inhibition. Sci Transl Med. 2018; 10(425). Epub 2018/01/26. https://doi.org/10.1126/scitranslmed.aao1613 PMID: 29367345.

71. Arulanandam R, Batenchuk C, Varette O, Zakaria C, Garcia V, Forbes NE, et al. Microtubule disruption synergizes with oncolytic virotherapy by inhibiting interferon translation and potentiating bystander killing. Nat Commun. 2015; 6:6410. Epub 2015/03/31. https://doi.org/10.1038/ncomms7410 PMID: 25817275.

72. Selman M, Rousso C, Bergeron A, Son HH, Krishnan R, El-Sayes NA, et al. Multi-modal Potentiation of Oncolytic Virotherapy by Vanadium Compounds. Mol Ther. 2018; 26(1):56–69. Epub 2017/11/28. https://doi.org/10.1016/j.ymthe.2017.10.014 PMID: 29175158; PubMed Central PMCID: PMC5763159.

73. Phan M, Watson MF, Alain T, Diallo JS. Oncolytic Viruses on Drugs: Achieving Higher Therapeutic Efficacy. ACS Infect Dis. 2018; 4(10):1448–67. Epub 2018/08/29. https://doi.org/10.1021/acsinfecdis.8b00144 PMID: 30152676.

74. Bergeron A, Kostenkova K, Selman M, Murakami HA, Owens E, Haribabu N, et al. Enhancement of oncolytic virotherapy by vanadium(V) dipicolinates. BioMetals. 2019; 32(3):545–61. https://doi.org/10.1007/s10534-019-00200-9 PMID: 31209680

75. Garza-Mayers AC, Miller KA, Russo BC, Nagda DV, Goldberg MB. Shigella flexneri regulation of ARF6 activation during bacterial entry via an IpgD-mediated positive feedback loop. mBio. 2015; 6(2):e02584. Epub 2015/03/05. https://doi.org/10.1128/mBio.02584-14 PMID: 25736891; PubMed Central PMCID: PMC4358011.

76. Mallo GV, Espina M, Smith AC, Terebiznik MR, Alemán A, Finlay BB, et al. SopB promotes phosphatidylinositol 3-phosphate formation on Salmonella vacuoles by recruiting Rab5 and Vps34. J Cell Biol. 2008; 182(4):741–52. Epub 2008/08/30. https://doi.org/10.1083/jcb.200804131 PMID: 18725540; PubMed Central PMCID: PMC2518712.

77. Carricaburu V, Lamia KA, Lo E, Favereaux L, Payrastre B, Cantley LC, et al. The phosphatidylinositol (PI)-5-phosphate 4-kinase type II enzyme controls insulin signaling by regulating PI-3,4,5-trisphosphate degradation. Proc Natl Acad Sci U S A. 2003; 100(17):9867–72. Epub 20030801. https://doi.org/10.1073/pnas.1734038100 PMID: 12897244; PubMed Central PMCID: PMC187868.

78. Chatterjee R, Chaudhuri D, Setty SRG, Chakravortty D. Deceiving the big eaters: Salmonella Typhimurium SopB subverts host cell xenophagy in macrophages via dual mechanisms. Microbes Infect. 2023; 25(6):105128. Epub 20230404. https://doi.org/10.1016/j.micinf.2023.105128 PMID: 37019426.

79. Radoshitzky SR, Pegoraro G, Chi XO, L DN, Chiang CY, Jozwick L, et al. siRNA Screen Identifies Trafficking Host Factors that Modulate Alphavirus Infection. PLoS Pathog. 2016; 12(3):e1005466. Epub 2016/04/01. https://doi.org/10.1371/journal.ppat.1005466 PMID: 27031835; PubMed Central PMCID: PMC4816540 and YC and JHK are employed by Tunnell Government Services, Inc. There are no patents, products in development or marketed products to declare. These employments do not alter our adherence to all the PLoS Pathogens policies on sharing data and materials, as detailed online in the guide for authors.

80. Van Huizen E, McInerney GM. Activation of the PI3K-AKT Pathway by Old World Alphaviruses. Cells. 2020; 9(4). Epub 2020/04/25. https://doi.org/10.3390/cells9040970 PMID: 32326388; PubMed Central PMCID: PMC7226951.

81. Wein T, Sorek R. Bacterial origins of human cell-autonomous innate immune mechanisms. Nat Rev Immunol. 2022; 22(10):629–38. Epub 20220408. https://doi.org/10.1038/s41577-022-00705-4 PMID: 35396464.

82. Doron S, Melamed S, Ofir G, Leavitt A, Lopatina A, Keren M, et al. Systematic discovery of antiphage defense systems in the microbial pangenome. Science. 2018; 359(6379). Epub 20180125. https://doi.org/10.1126/science.aar4120 PMID: 29371424; PubMed Central PMCID: PMC6387622.

83. Ledvina HE, Whiteley AT. Conservation and similarity of bacterial and eukaryotic innate immunity. Nat Rev Microbiol. 2024. Epub 20240228. https://doi.org/10.1038/s41579-024-01017-1 PMID: 38418927.

84. Jacob F, Vernaldi S, Maekawa T. Evolution and Conservation of Plant NLR Functions. Front Immunol. 2013; 4:297. Epub 2013/10/05. https://doi.org/10.3389/fimmu.2013.00297 PMID: 24093022; PubMed Central PMCID: PMC3782705.

85. Gomez-Valero L, Rusniok C, Carson D, Mondino S, Pérez-Cobas AE, Rolando M, et al. More than 18,000 effectors in the Legionella genus genome provide multiple, independent combinations for replication in human cells. Proc Natl Acad Sci U S A. 2019; 116(6):2265–73. Epub 20190118. https://doi.org/10.1073/pnas.1808016116 PMID: 30659146; PubMed Central PMCID: PMC6369783.

86. Chen J, Byun H, She Q, Liu Z, Ruggeberg KG, Pu Q, et al. S-Nitrosylation of the virulence regulator AphB promotes Vibrio cholerae pathogenesis. PLoS Pathog. 2022; 18(6):e1010581. Epub 20220617. https://doi.org/10.1371/journal.ppat.1010581 PMID: 35714156; PubMed Central PMCID: PMC9246220.

87. Kwon JJ, Hajian B, Bian Y, Young LC, Amor AJ, Fuller JR, et al. Structure-function analysis of the SHOC2-MRAS-PP1C holophosphatase complex. Nature. 2022; 609(7926):408–15. Epub 20220713. https://doi.org/10.1038/s41586-022-04928-2 PMID: 35831509; PubMed Central PMCID: PMC9694338.

88. Rodriguez-Viciana P, Oses-Prieto J, Burlingame A, Fried M, McCormick F. A Phosphatase Holoenzyme Comprised of Shoc2/Sur8 and the Catalytic Subunit of PP1 Functions as an M-Ras Effector to Modulate Raf Activity. Molecular Cell. 2006; 22(2):217–30. https://doi.org/10.1016/j.molcel.2006.03.027 PMID: 16630891

89. Zhao BR, Wang XX, Wang XW. Shoc2 recognizes bacterial flagellin and mediates antibacterial Erk/Stat signaling in an invertebrate. PLoS Pathog. 2022; 18(1):e1010253. Epub 2022/01/25. https://doi.org/10.1371/journal.ppat.1010253 PMID: 35073369; PubMed Central PMCID: PMC8812994.

90. Zhu Y, Wang WL, Yu D, Ouyang Q, Lu Y, Mao Y. Structural mechanism for nucleotide-driven remodeling of the AAA-ATPase unfoldase in the activated human 26S proteasome. Nature Communications. 2018; 9(1):1360. https://doi.org/10.1038/s41467-018-03785-w PMID: 29636472

91. Köhler A, Cascio P, Leggett DS, Woo KM, Goldberg AL, Finley D. The Axial Channel of the Proteasome Core Particle Is Gated by the Rpt2 ATPase and Controls Both Substrate Entry and Product Release. Molecular Cell. 2001; 7(6):1143–52. https://doi.org/10.1016/s1097-2765(01)00274-x PMID: 11430818

92. Beckwith R, Estrin E, Worden EJ, Martin A. Reconstitution of the 26S proteasome reveals functional asymmetries in its AAA+ unfoldase. Nature Structural & Molecular Biology. 2013; 20(10):1164–72. https://doi.org/10.1038/nsmb.2659 PMID: 24013205

93. Jang ER, Jang H, Shi P, Popa G, Jeoung M, Galperin E. Spatial control of Shoc2-scaffold-mediated ERK1/2 signaling requires remodeling activity of the ATPase PSMC5. J Cell Sci. 2015; 128(23):4428–41. Epub 2015/11/01. https://doi.org/10.1242/jcs.177543 PMID: 26519477; PubMed Central PMCID: PMC4712819.

94. Bi W, Bao K, Zhou X, Deng Y, Li X, Zhang J, et al. PSMC5 regulates microglial polarization and activation in LPS-induced cognitive deficits and motor impairments by interacting with TLR4. Journal of Neuroinflammation. 2023; 20(1):277. https://doi.org/10.1186/s12974-023-02904-9 PMID: 38001534

95. Sun C, Desch K, Nassim-Assir B, Giandomenico SL, Nemcova P, Langer JD, et al. An abundance of free regulatory (19S) proteasome particles regulates neuronal synapses. Science. 2023; 380(6647):eadf2018. https://doi.org/10.1126/science.adf2018 PMID: 37228199

96. Rigante D, Leoni C, Onesimo R, Giorgio V, Trevisan V, Zampino G. Aberrant N-myristoylation as a prelude to autoimmune manifestations in patients with SHOC2 mutations. Autoimmun Rev. 2023; 22 (11):103462. Epub 20231002. https://doi.org/10.1016/j.autrev.2023.103462 PMID: 37793491.

97. Haertle L, Buenache N, Cuesta Hernández HN, Simicek M, Snaurova R, Rapado I, et al. Genetic Alterations in Members of the Proteasome 26S Subunit, AAA-ATPase (PSMC) Gene Family in the Light of Proteasome Inhibitor Resistance in Multiple Myeloma. Cancers (Basel). 2023; 15(2). Epub 20230115. https://doi.org/10.3390/cancers15020532 PMID: 36672481; PubMed Central PMCID: PMC9856285.

98. Tychhon B, Allen JC, Gonzalez MA, Olivas IM, Solecki JP, Keivan M, et al. The prognostic value of 19S ATPase proteasome subunits in acute myeloid leukemia and other forms of cancer. Front Med (Lausanne). 2023; 10:1209425. Epub 2023/07/28. https://doi.org/10.3389/fmed.2023.1209425 PMID: 37502358; PubMed Central PMCID: PMC10371016.

99. Liu L, Hu C, Chen Z, Zhu S, Zhu L. Co-Occurring Thrombotic Thrombocytopenic Purpura and Autoimmune Hemolytic Anemia in a Child Carrying the Pathogenic SHOC2 c.4A>G (p.Ser2Gly) Variant. Am J Case Rep. 2023; 24:e942377. Epub 20231129. https://doi.org/10.12659/ajcr.942377 PMID: 38019730; PubMed Central PMCID: PMC10697549.

100. Kwon JJ, Hahn WC. A Leucine-Rich Repeat Protein Provides a SHOC2 the RAS Circuit: a Structure-Function Perspective. Mol Cell Biol. 2021; 41(4). Epub 2021/02/03. https://doi.org/10.1128/mcb.00627-20 PMID: 33526449; PubMed Central PMCID: PMC8088128.

101. Xie CM, Tan M, Lin XT, Wu D, Jiang Y, Tan Y, et al. The FBXW7-SHOC2-Raptor Axis Controls the Cross-Talks between the RAS-ERK and mTORC1 Signaling Pathways. Cell Rep. 2019; 26(11):3037–50 e4. Epub 2019/03/14. https://doi.org/10.1016/j.celrep.2019.02.052 PMID: 30865892; PubMed Central PMCID: PMC6503676.

102. Weigele BA, Orchard RC, Jimenez A, Cox GW, Alto NM. A systematic exploration of the interactions between bacterial effector proteins and host cell membranes. Nat Commun. 2017; 8(1):532. Epub 2017/09/16. https://doi.org/10.1038/s41467-017-00700-7 PMID: 28912547; PubMed Central PMCID: PMC5599653.

103. Minor W, Cymborowski M, Otwinowski Z, Chruszcz M. HKL-3000: the integration of data reduction and structure solution—from diffraction images to an initial model in minutes. Acta Crystallogr D Biol Crystallogr. 2006; 62(Pt 8):859–66. Epub 20060718. https://doi.org/10.1107/s0907444906019949 PMID: 16855301.

104. Domingo E, García-Crespo C, Lobo-Vega R, Perales C. Mutation Rates, Mutation Frequencies, and Proofreading-Repair Activities in RNA Virus Genetics. Viruses. 2021; 13(9). Epub 2021/09/29. https://doi.org/10.3390/v13091882 PMID: 34578463; PubMed Central PMCID: PMC8473064.

105. Otwinowski Z, Borek D, Majewski W, Minor W. Multiparametric scaling of diffraction intensities. Acta Crystallogr A. 2003; 59(Pt 3):228–34. Epub 20030425. https://doi.org/10.1107/s0108767303005488 PMID: 12714773.

106. Borek D, Dauter Z, Otwinowski Z. Identification of patterns in diffraction intensities affected by radiation exposure. J Synchrotron Radiat. 2013; 20(Pt 1):37–48. Epub 20121206. https://doi.org/10.1107/S0909049512048807 PMID: 23254654; PubMed Central PMCID: PMC3526920.

107. Borek D, Cymborowski M, Machius M, Minor W, Otwinowski Z. Diffraction data analysis in the presence of radiation damage. Acta Crystallogr D Biol Crystallogr. 2010; 66(Pt 4):426–36. Epub 20100324. https://doi.org/10.1107/S0907444909040177 PMID: 20382996; PubMed Central PMCID: PMC2852307.

108. Adams PD, Afonine PV, Bunkóczi G, Chen VB, Davis IW, Echols N, et al. PHENIX: a comprehensive Python-based system for macromolecular structure solution. Acta Crystallogr D Biol Crystallogr. 2010; 66(Pt 2):213–21. Epub 20100122. https://doi.org/10.1107/s0907444909052925 PMID: 20124702; PubMed Central PMCID: PMC2815670.

109. Emsley P, Lohkamp B, Scott WG, Cowtan K. Features and development of Coot. Acta Crystallogr D Biol Crystallogr. 2010; 66(Pt 4):486–501. Epub 20100324. https://doi.org/10.1107/S0907444910007493 PMID: 20383002; PubMed Central PMCID: PMC2852313.

110. Hansen JM, de Jong MF, Wu Q, Zhang L-S, Heisler DB, Alto LT, et al. Pathogenic ubiquitination of GSDMB inhibits NK cell bactericidal functions. Cell. 2021; 184(12):3178–91.e18. https://doi.org/10.1016/j.cell.2021.04.036 PMID: 34022140